VIBRATION ISOLATION MODULE DESIGN FOR A TOWED ARRAY

A THESIS SUBMITTED TO
THE GRADUATE SCHOOL OF NATURAL AND APPLIED SCIENCES
OF
MIDDLE EAST TECHNICAL UNIVERSITY

BY

ÖMER BATMAZ

IN PARTIAL FULFILLMENT OF THE REQUIREMENTS
FOR
THE DEGREE OF MASTER OF SCIENCE
IN
MECHANICAL ENGINEERING

FEBRUARY 2014

Approval of the thesis:

VIBRATION ISOLATION MODULE DESIGN FOR A TOWED ARRAY

submitted by **ÖMER BATMAZ** in partial fulfillment of the requirements for the degree of **Master of Science in Mechanical Engineering Department, Middle East Technical University** by,

Prof. Dr. Canan ÖZGEN _____
Dean, Graduate School of **Natural and Applied Sciences**

Prof. Dr. Suha ORAL _____
Head of Department, **Mechanical Engineering**

Prof. Dr. Mehmet ÇALIŞKAN _____
Supervisor, **Mechanical Engineering Dept., METU**

Assist. Prof. Gökhan O. ÖZGEN _____
Co-Supervisor, **Mechanical Engineering Dept., METU**

Examining Committee Members:

Assoc. Prof. Ender CİĞEROĞLU _____
Mechanical Engineering Dept., METU

Prof. Dr. Mehmet ÇALIŞKAN _____
Mechanical Engineering Dept., METU

Assist. Prof. Gökhan O. ÖZGEN _____
Mechanical Engineering Dept., METU

Assist. Prof. Kıvanç AZGIN _____
Mechanical Engineering Dept., METU

Dr. Murat AYKAN _____
ASELSAN INC.

Date: 19.02.2014

I hereby declare that all information in this document has been obtained and presented in accordance with academic rules and ethical conduct. I also declare that, as required by these rules and conduct, I have fully cited and referenced all material and results that are not original to this work.

Name, Last name : Ömer BATMAZ

Signature :

ABSTRACT

VIBRATION ISOLATION MODULE FOR A TOWED ARRAY

BATMAZ, Ömer
M. Sc., Department of Mechanical Engineering
Supervisor : Prof. Dr. Mehmet ÇALIŞKAN
Co-Supervisor : Assist. Prof. Gökhan O. ÖZGEN

February 2014, 108 pages

Today, towed arrays are widely utilized in both civilian and military applications such as oil/gas explorations or submarine/torpedo detections under the water. Hydrophones are linearly arranged in the acoustic section of a towed array. These hydrophones convert the reverberated acoustical signals from targets into electrical signals and send them to the data acquisition center on the tow vessel. Any kind of noise on hydrophones negatively affects the performance of the array during operation. Vibrations coming from the tow cable and drogue rope are important noise mechanisms; especially at low working frequencies and tow speeds. In order to suppress these vibrations from the hydrophone section and hence increase the signal-to-noise ratio of the array, vibration isolation modules (VIMs) are attached to forward and aft ends of the hydrophone section. During the design phase of the VIM, it is highly desirable to be able to predict the dynamic behavior of the module. Consequently, this study was undertaken in order to determine the modal characteristics of the VIM. Firstly, Myklestad's Method for bending was used to build up mathematical model of the VIM. Since the VIM structure is not slender

and there is always considerable drag force on the VIM during operation, shear effects and variable tension force were implemented to the method. A vertically hung VIM was tested to provide both free-free boundary condition and variable tension. The study was concluded with a thorough comparison of the theoretical and experimental results in order to evaluate the effectiveness of the modified method.

Keywords: Vibration Isolation Module (VIM), Myklestad's Method, Towed Array

ÖZ

ÇEKİLİ DİZİN İÇİN TİTREŞİM İZOLASYON MODÜLÜ TASARIMI

BATMAZ, Ömer
Yüksek Lisans, Makina Mühendisliği Bölümü
Tez Yöneticisi : Prof. Dr. Mehmet ÇALIŞKAN
Ortak Tez Yöneticisi : Yrd. Doç. Gökhan O.ÖZGEN

Şubat 2014, 108 Sayfa

Günümüzde çekili dizinler, sualtı doğalgaz/petrol araştırmaları veya denizaltı/torpido tespiti gibi sivil ve askeri uygulamalarda yaygın bir şekilde kullanılmaktadır. Çekili dizinin akustik bölümünde doğrusal olarak dizilmiş hidrofonlar bulunmaktadır. Bu hidrofonların görevi hedeften yansıyan ses dalgalarını elektriksel sinyallere dönüştürmek ve bu sinyalleri çekici deniz aracı üzerinde bulunan veri işleme merkezine göndermektir. Operasyon sırasında hidrofonlar üzerinde oluşabilecek herhangi bir gürültü, dizin performansını olumsuz yönde etkileyecektir. Çekme kablosu ve kuyruk ipinden gelen titreşimler önemli gürültü mekanizmalarıdır. Titreşim kaynaklı gürültüler özellikle düşük çalışma frekansları ve çekme hızlarında etkili olmaktadır. Gürültü kaynağı olan bu titreşimleri hidrofonların olduğu bölümden uzak tutmak ve böylece sinyal-gürültü oranını arttırmak için akustik bölümün ön ve arka ucuna titreşim izolasyon modülleri (TİM) eklenmektedir. TİM'in dinamik davranışının tasarım aşamasında belirlenebiliyor olması gerekmektedir. Bu sebepten, TİM'in modal karakterinin belirlenmesi için bu çalışma ele alınmıştır. İlk olarak Myklestad metodu

kullanılarak TİM'in matematiksel modeli oluşturulmuştur. TİM ince-uzun bir yapıda olmadığından kesme etkileri metoda eklenmiştir. Operasyon boyunca TİM üzerinde sürükleme kuvveti oluşacağından, değişken çekme kuvveti de Myklestad metoduna ayrıca uygulanmıştır. Düşey olarak asılmış TİM ile testler yapılmıştır. Böylece hem serbest sınır koşulları hem de TİM üzerinde değişken gerilim kuvveti sağlanmıştır. Oluşturulan matematiksel modelin geçerliliğini değerlendirmek için bu çalışma sonunda teorik sonuçlar ile test sonuçları esaslı bir şekilde karşılaştırılmıştır.

Anahtar Kelimeler: Titreşim İzolasyon Modülü, Myklestad Metodu, Çekili Dizin

To My Lovely Wife

ACKNOWLEDGEMENTS

First of all, I would like to offer my special thanks to my supervisor Prof. Dr. Mehmet Çalışkan and co-supervisor Assist. Prof. Gökhan O. Özgen for their unsurpassed guidance, criticism and continued support throughout this study.

I would like to express my gratitude to Dr. Murat Aykan, Özge Mencek, Necati Karaismailoğlu, Taner Karagöz and Yiğit Özpak for their assistance and patience.

Also, I am grateful to my company ASELSAN Inc. for supporting my work and providing me test facilities.

Special thanks to my mother, Cemile and my father, İbrahim. Your prayers for me were what sustained me thus far.

Finally, this thesis could not have been completed without supporting of my generous wife, Beyza Batmaz. Thank you very much for allowing me time away from you to research and write.

TABLE OF CONTENTS

LIST OF TABLES

TABLES

LIST OF FIGURES

LIST OF SYMBOLS

A	Cross-section area
E	Elastic modulus (Modulus of elasticity)
E^*	Complex dynamic modulus
E_1	Storage modulus
E_2	Loss modulus
G	Shear modulus (Modulus of rigidity)
I	Area moment of inertia
k	Spring constant
M	Bending moment
m	Mass
Q, V	Shear force
T	Period
t	Time
y	Deflection in transverse direction
x	Horizontal distance
β	Slope due to shear
δ	Phase
ε	Strain
ε_0	Amplitude of the strain
η	Loss factor
κ	Shear coefficient
λ	Eigen value
μ	Viscous constant
ν	Poisson`s ratio
ρ	Density
σ	Stress
σ_0	Amplitude of the stress

ψ	Slope due to bending
ω	Angular frequency
ω_n	*n*th natural frequency
[F]	Field transfer matrix
[P]	Point transfer matrix
[S]	State vector
[T]	Transfer matrix
[U]	Overall transfer matrix

ABBREVIATIONS

DMA	Dynamic Mechanical Analysis
FEM	Finite Element Method
FFT	Fast Fourier Transform
FRF	Frequency Response Function
MIMO	Multiple Input Multiple Output
MISO	Multiple Input Single Output
SIMO	Single Input Multiple Output
SLS	Standard Linear Solid
TMM	Transfer Matrix Method
VIM	Vibration Isolation Module

CHAPTER 1

INTRODUCTION

This chapter of this thesis covers brief information about towed arrays and area of their usage. After that, negative effects of noise on towed array performance and some most important noise sources will be explained. Since the vibration is the main topic of the thesis, vibration-induced noise among the noise sources will be explained in a little more detail. Additionally, to be able to minimize negative effects of vibration on the array, importance of VIM (Vibration Isolation Module) will be mentioned. Finally, objective of the thesis and thesis organization will be given at the end of this chapter.

1.1 What is the Towed Array?

A towed array is a passive sonar system which is deployed as a line array and towed behind a surface ship or a submarine (Figure 1.1). Passive means that the towed array only gathers radiated or reflected acoustic signals from undersea objects or structures.

Previously, the towed arrays were widely utilized for unmilitary applications which are oil/gas/valuable minerals explorations or geophysical studies on sea bottom. In this kind of applications, low-frequency acoustic waves are generated by a high pressure air gun and travel towards sea bottom. The characteristics of generated waves change according to acoustic impedance of the obstacles when the waves hit them. Reverberated waves then travel back and are collected by towed array. The acoustic data coming from towed array is converted into useful information about underwater natural resources or landscape of the sea bottom.

Generally, very low frequencies, lower than 120 Hz, are used in civilian applications [1].

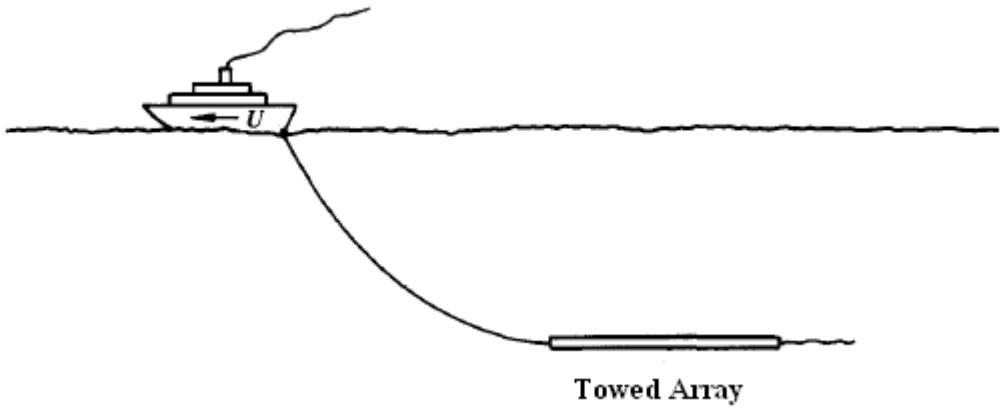

Figure 1.1 A Simple illustration of surface ship and towed array [2]

Towed arrays appeared in military applications in 1960s. They are intended for detection and identification of submarines and torpedoes. Although the working principles of all towed arrays are similar, there are some noticeable distinctions in design for naval applications. Working frequency range can be specified as the most significant differences. Upper frequency limit of military towed arrays goes up to tens of kHz.

Today, the towed arrays are irrevocable equipments for both sea bottom explorations and threat detections. Abilities and properties of towed arrays have been advanced day by day with developing technology.

A towed array is composed of many subsections, namely tow cable, forward VIM, non-acoustic module, hydrophone section (acoustic section), aft VIM and drogue

rope, in sequence. An illustration of a typical towed array is given in Figure 1.2. In some special case, extra sections can be integrated to array, as well.

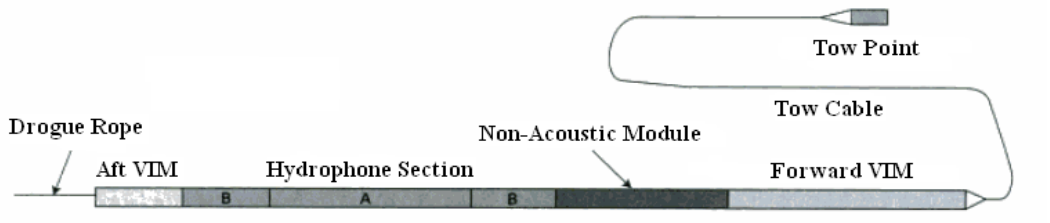

Figure 1.2 Components of a typical towed array [3]

Tow cable is used to tow whole array assembly in the water. It is the only component which physically contacts with tow vessel or submarine. It contains steel wire mesh to be able to stand against drag force without any failure and both power and data cables inside. Also, it is the longest part of the array and the length of the tow cable is variable according to desired operation depth or tow vessel speed.

Forward VIM is located just after the tow cable. Vibration and strumming noise coming from tow cable are aimed to be absorbed by this section. Likewise the forward VIM, function of the aft VIM is to attenuate vibration due to whip-like action of the drogue rope. Generally, physical properties of both VIMs are similar to hydrophone section but various VIMs have been designed so far to increase the extent of vibration isolation.

Non-acoustic module does not contain any sensor. In many of applications, it is integrated into hydrophone section. Specialized electrical devices such as analog-to-digital converters and amplifiers lie in here.

Hydrophone section is the most crucial component of the towed array. It is composed of hundreds of hydrophones which are set linearly inside a plastic hose. The hose is filled with low density oil to make the array neutrally buoyant. This section converts the acoustical signals into electrical signals and sends them to the data acquisition center on the tow vessel. Interested frequency range and desired directional resolution define the hydrophone section length. There might be more than one hydrophone arrangement in the plastic hose because each arrangement deals with distinctive frequency bands.

Drogue rope is the last component that is connected to the end of the aft VIM. Being horizontal during operation strongly affects the performance of the hydrophone section. So that, drogue rope is added in order to increase drag force and straighten the array.

Measurement precision of a towed array definitely depends on the noise coming out within the desired detection spectrum range. Sources of the unwanted noise on array could be environmental or operational factors during towing action. In the next section, noise sources one of which is, of course, vibration induced noise will be explained under the four main titles in short.

1.2 Causes of Noise on Towed Array

Any kind of noise on hydrophones deteriorates performance of the array during operation. Acoustic pressure signals received by hydrophones are not strong enough. Additionally, impedances of the hydrophones are also high as an inherent property. As a result of these conditions, hydrophones are able to generate the signal at low level only [4]. So, noise source should be carefully investigated in order to minimize noise effects on hydrophones and increase the signal to noise ratio.

Prediction of the noise on array is not easy to handle theoretically. Empirical studies have always guided the researchers from past to present. So, all probable

factors, such as length of the tow cable, distance between hydrophones, propeller noise, depth of operation, etc., have been examined one by one and their effects on noise levels are approximately identified.

Although many mechanisms different from each other induce noise on the towed array, they still can be classified into four groups, namely ambient noise, radiated noise, flow noise and vibration noise. Effects of these noise mechanisms highly depend on the towing speed and frequency. This means that while one of mechanisms is dominant at a specified towing speed and frequency, this mechanism disappears or can be suppressed by other mechanisms when the speed is changed. A related chart summarizing the dependency is given in Figure 1.3.

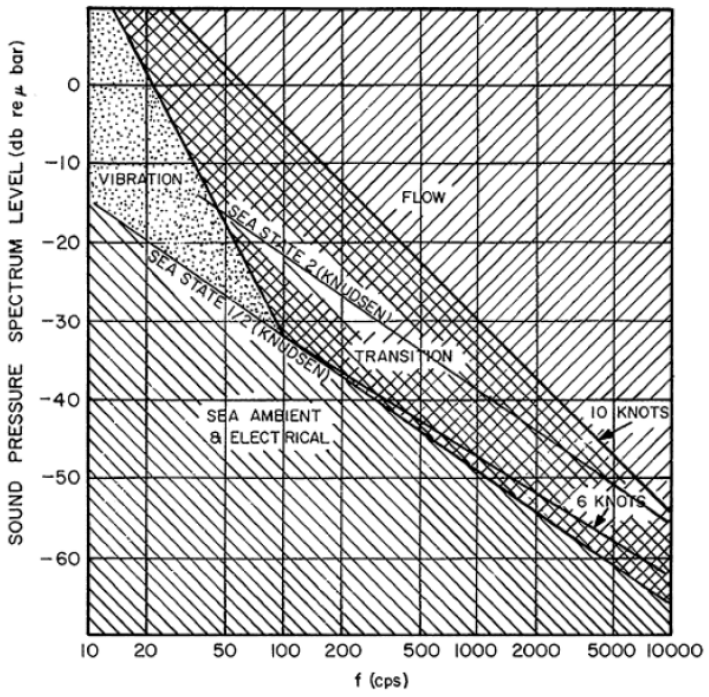

Figure 1.3 Classification of the noise for a single hydrophone in the array according to towing speed and frequency [5]

One can interpret from the above chart that noise at low towing speeds is caused by sea ambient and vibration but flow noise becomes dominant as towing speed increases.

1.2.1 Ambient Noise

As stated before, sea ambient noise is effective at low towing speeds and has a wide frequency range. Many studies have been conducted to determine the sea ambient noise from 1Hz to 100 kHz, so far. As a result of these studies, sources of sea ambient noise and their frequency bands are discovered. Also, it should be noted that amplitude of the ambient noise depends on depth of the water. Noise levels in shallow-water are generally higher than in deep waters [6].

Surface waves are indicated as ambient noise sources. Magnitude of wind speed with the height of the surface waves are specified by using sea-state scale. Knudsen spectrum is a well-known method to understand the relation between sea-states, directly surface waves, and ambient noise levels. As well as surface waves, rain is another noise source related with weather conditions. In case of extremely heavy rain, several tens of dB increase can be observed in noise levels. Because of that tides create pressure fluctuation in the sea, they are another ambient noise source. However, noise from tides contains very low frequency components which are far away from operation frequency most of the time. Instability of the seabed also generates undesired noise on the arrays. Moreover volcanic eruptions and earth quakes contribute to formation of this kind of noise. Since, these seismic noises appear at very low frequency region, they are generally suppressed by other noises. Turbulence due to gulf or vortex is accepted as a noise source for the sea ambient noise, as well. However, sea turbulence originating noise is dramatically attenuated with distance so that it is not a critical disturbance for array performance. Lastly, ship traffic vicinity of tow operation is an important noise source. Frequency characteristics of ship traffic noise lies from 50 Hz to 500 Hz but it is dominant at around 100 Hz. All these above noise are caricaturized in Figure 1.4.

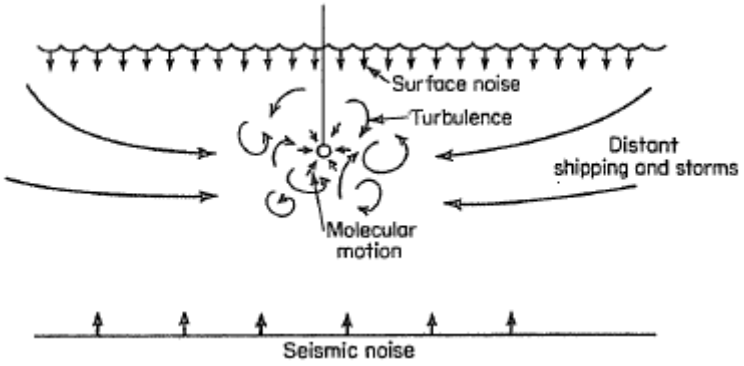

Figure 1.4 Sources of sea ambient noise [7]

As a result, noise from the surface waves and the ship traffic should be taken seriously among ambient noise sources because of that they mostly exist in the range of operation frequency.

1.2.2 Radiated Noise

Radiated noise phenomenon can be confused with ambient noise but noises propagating from surface ship or submarine to which the array is connected are investigated under this title. Machinery on hull, propeller and movement of surface ship or submarine are potential noise sources. According to noise source, frequency characteristics of the radiated noise can be in form of broadband or tonal.

Vibrations of machines on hull create unwanted noise in the water. Internal combustion engines, gear assemblies, pumps, generators and all mechanical irregularities are the source of machinery noise. Machinery noise is a kind of low level broadband noise with powerful tonal components. Unlike machinery noise, propeller noise is transmitted into water directly. Three mechanisms which are blade rate, cavitation and blade singing take part in developing of propeller noise. While blade rate and blade singing effects are observed as tonal noise, cavitation

forms broadband noise at spectrum. The last element of radiated noise is hydrodynamic noise. Motion depended turbulent layer excites the hull and propeller so that structural born noise is induced. Nevertheless, hydrodynamic noise pales beside machinery and propeller noise.

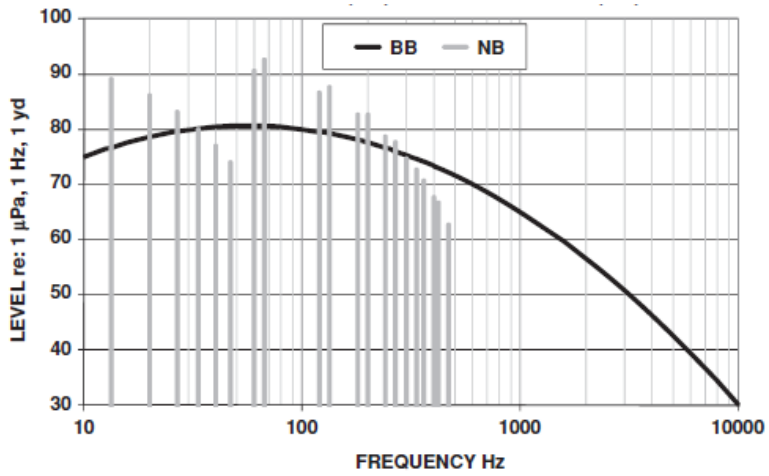

Figure 1.5 Radiated noise components of a surface ship [8]

Radiated noise spectrum of a surface ship is shown in Figure 1.5. Broadband noise and tonal noises are assigned individually. It can be obviously seen from the graph that levels of some tonal noises lie under the broadband noise level and so they disappear.

1.2.3 Flow Noise

During the towing action, a turbulent boundary layer develops around of the array because of the relative motion Figure 1.6. Pressure fluctuations as a nature of turbulence are carried inside the array by some mechanisms and they are turned into unwanted noise at the output of the hydrophones. So, this sort of noise is

called as flow noise. Mostly, performances of the arrays are assigned according to flow noise because of the fact that high frequency components of flow noise are also significant when it is compared with other noise sources. They are effective in broad spectrum, especially at high towing speeds.

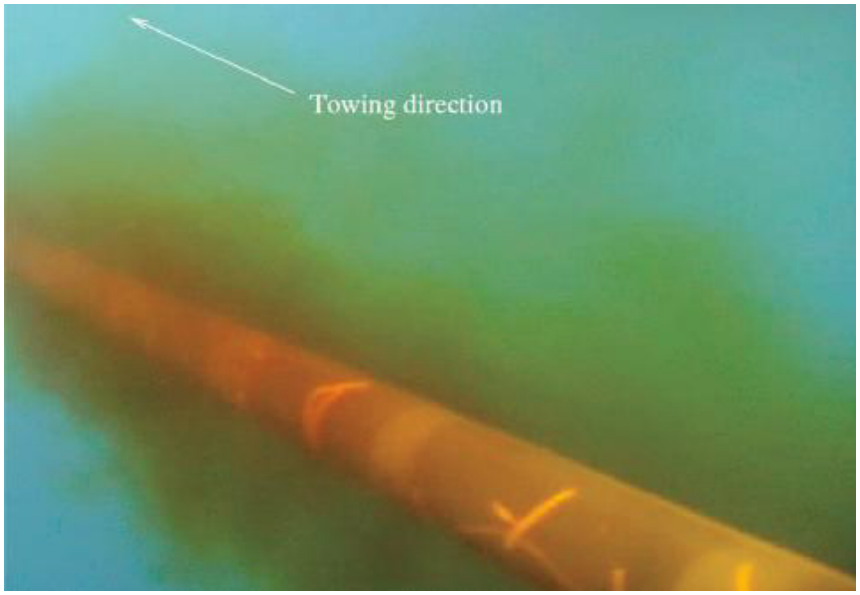

Figure 1.6 Turbulent boundary layer around a tow cable [9]

However, disturbance effects of flow noise on collected data could be filter out by taking statistical averages or mechanical precautions some like adjusting the distance of hydrophones or minimizing the contacts of the hydrophones to the outer hose.

1.2.4 Vibration Noise

As is seen in Figure 1.3, vibration noise cannot be disregarded at low frequency range because it has the highest noise level during low speed towing actions.

Anyhow hydrophones in the array are designed to sense pressure waves; they are inherently affected by vibration on their body, as well. So, any vibration source can be indicated as a vibration noise source directly.

Turbulent boundary layer does not only cause flow noise mentioned before but also it is the one of main reasons of vibration on the array. Another crucial vibration source is vortex shedding of the tow cable. It is the case of boundary layer separation as known. After separation, vortices are developed and they ruin the stable pressure distribution over the tow cable so that unequal lifting force due to pressure instability makes the cable oscillate. Some portion of the vibration on the cable is attenuated; however, the rest stands themselves out as erroneous data at the output of the hydrophones. At the same time, connection of the tow cable to the deck is almost rigid so machine induced vibration becomes a vibration source for the array. That is, the hull vibration is conveyed up to the hydrophones along the cable and can corrupt their output data. Additionally, instabilities on both drag force and towing speed can be shown as another vibration source. Finally, fluttering of the drogue rope may causes oscillation of the components.

The notable vibration noise source among above sources is admittedly vibration of the tow cable. Two types of vibration which are transverse vibration and longitudinal vibration come into existence on the cable and these are naturally transferred to the hydrophone section. According to occurrence plane, transverse vibration is examined as being in yaw and pitch directions Figure 1.7. Vortex shedding is especially the main reason of the transverse cable vibration. Although vortex frequencies cannot exceed 100 Hz, vibration noise must be taken into consideration in low frequency researches.

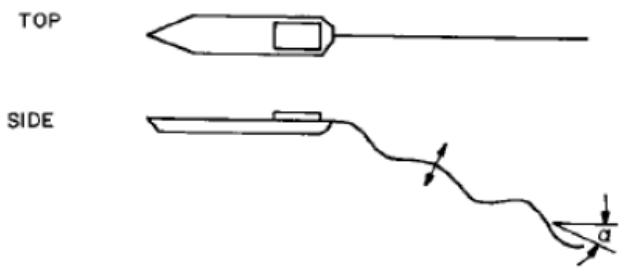

(a)

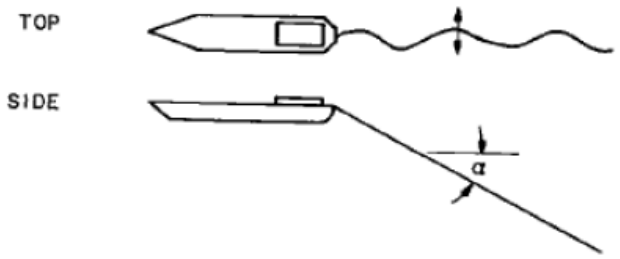

(b)

Figure 1.7 Vibration of the tow cable in (a) pitch and (b) yaw directions [10]

In terms of longitudinal vibrations, instabilities in flow and some mechanisms related with transverse vibration can be accepted as their sources. These vibrations are quite responsive to damping factor of the system; that is, their attenuation rates increase sharply after 50 Hz when damping factor goes up [10].

1.3 Vibration Isolation Module (VIM)

The negative effect of the all above vibrations can be diminished by cutting of the direct connection of the tow cable and drogue rope with hydrophone section. Thus, VIMs have been interposed between these components. By changing the

mechanical properties of VIM`s, optimum attenuation may be achieved at desired frequency ranges.

Although many different VIM structures have been used in marine applications, classical VIMs comprising of elastic outer hose, inner fluid, rigid spacers, internal strength members and termination parts have common use because of their production costs. According to its location, VIM may contain power and data cables, as well. Figure 1.8 demonstrates the structure of a classical VIM.

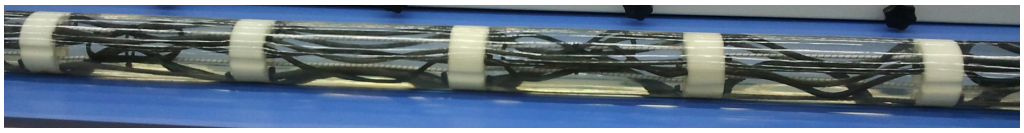

Figure 1.8 Structure of a classical VIM

Elastic hose holds the all components together and protects them from external factors. It is generally produced from flexible materials like polyurethane. Hose is filled by internal fluid whose density is lower than water to achieve neutral buoyancy. Termination parts are attached to each end to conserve inner fluid inside the hose and provide connection interface. In case of any excessive tension, strength members lying from one to other prevent the damage of the VIM. Rigid spacers are put with spacing into the VIM to increase the bending stiffness for desired operation conditions. They also protect the power and data cable when excessive bending occurs.

1.4 Objectives of the Thesis

As mentioned before, it is very important to minimize vibration effects to be able to increase signal to noise ratio of the hydrophone section at low or moderate

towing speeds. Most of the vibrational disturbances arrive to hydrophones through the medium of tow cable and drogue rope. That's why, vibration isolation modules (VIMs) are extensively placed to the both forward and aft ends of the hydrophone section. In the design stage, dynamic behavior of these additional components should be predictable to implement the optimum solution against to vibration problem. Therefore, providing a useful and simple theoretical method to guide design of the VIMs on towed arrays is the motivation of this study.

The main objective of this thesis is to propose an analytical method for the multicomponent VIM structure in order to define its dynamic behavior, especially natural frequencies. Verification of the proposed method by performing experimental works is another goal of the study.

1.5 Scope of the Thesis

The outline of the thesis as follows:

In Chapter 2, patented VIM applications from literature are presented. Their structural properties which are different than each other are mentioned briefly. Additionally, studies on dynamic behavior of slender structures inside water are given in this chapter.

In Chapter 3, basic concepts about beam vibration and dynamic modulus of viscoelastic materials are given because hose of the VIM is a viscoelastic. Furthermore, it is stated here that Myklestad`s Method is utilized to define dynamic behavior of the VIM. After explain the simple form of this method, modified form which includes shear deformation and variable tension force in order to simulate real conditions of the VIM is introduced in detail.

In Chapter 4, the modal test technique which is used during test of the VIM sample is explained. The test setup and procedure are also presented. Lastly, test results of the VIM conclude this chapter.

In Chapter 5, modified Myklestad`s Method is verified by applying seven different boundary conditions. Natural frequencies obtained from the new method are compared with the Finite Element Method (FEM) results. After verification procedure, a solution is performed to find the first three bending natural frequency of the tested VIM sample by using new method. Additionally, comparison between the theoretical results and the experimental results of the VIM sample are presented. Valuable comments on results are expressed.

In Chapter 6, all study is summarized with remarkable conclusions and some suggestions about future works are stated under the summary and conclusions title.

CHAPTER 2

LITERATURE SURVEY

In this chapter, VIMs and VIM-like products which are used to attenuate vibration level on hydrophone side of the towed array will be examined under the first title. In addition, second part mentions various mathematical models used to define dynamics of cylindrical structures interacting with the water, such as hoses and cables.

2.1 Patented VIMs in Marine Applications

When the towed sonar arrays are investigated in detail, VIMs always exist as an irrevocable component of the systems.

Miller et al. [11] invented a VIM composed of nylon cords, flexible outer and inner envelope, rubber filler material between envelopes, viscous jelly filler inside the inner sheath and centered braided rope which has high braking strength. Function of the nylon cords is to withstand the moderate drag force related with fluid-array interaction. Rubber filler material damps the vibration and noise which are transferred from towing cable to nylon cords. Centered braided rope becomes active when the length of the VIM reaches the certain limits. Main reason of length change is increasing in towing speed which means increasing in drag force. Under the high tow speed, tight centered braided rope could increase the transmission of the cable vibration. However, they stated that at high speed flow noise will suppress the strumming noise. (Figure 2.1)

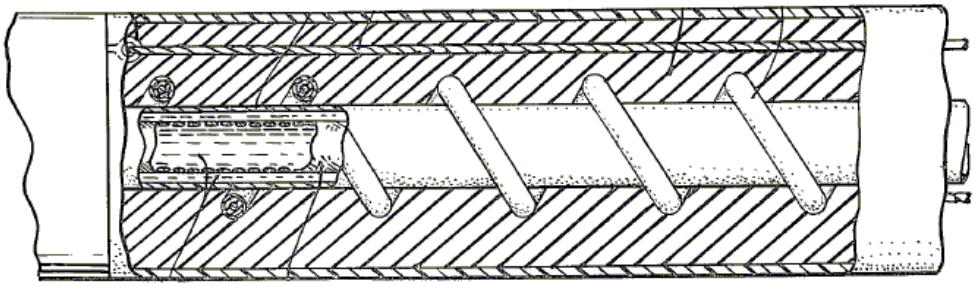

Figure 2.1 Cross section view of the Miller`s invention [11]

Using nylon ropes may expose negative effect on assembly of VIM and its vibration attenuation characteristic. It is difficult to fasten all nylon ropes one end to other with the same tension. Also, when nylon ropes reach their elastic limits, VIM will be work as an only connection element between tow cable and hydrophone section. By this way, elastic limit of nylon ropes determines the frequency range where VIM is effective. Appling [12] get these ropes out from his VIM design. This design includes only one braided aramid fiber rope with damping chambers at some intervals and polyurethane spacers. Length of the chambers, filler material inside them and space between spacers directly affect the vibration impedance of VIM. By changing these parameters, VIM for desired frequency range vibration isolation can be built up. Figure 2.2

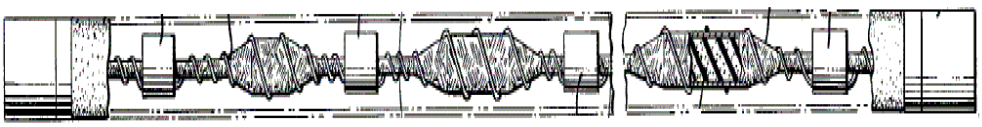

Figure 2.2 View of Appling`s invention [12]

Vibration attenuation mechanism of VIMs differs from each other. McGowan and McCulloch [13] redounded attenuation property of VIM by using spacers contact with outer hose. Outer hose is selected from polyurethane material and filled with neutral buoyancy fluid, too. Spacers are located on elastic main rope with special technique. At excessive tension situations, spacer can move on elastic main rope so that, unwanted stress concentration on rope would be eliminated. By touching to outer hose, spacers act as a bridge between outer hose and elastic main rope. In other words, vibration or strumming noise on main rope will be transferred to outer hose and vibration from out of the hose will conversely transferred to main rope by means of spacers. (Figure 2.3)

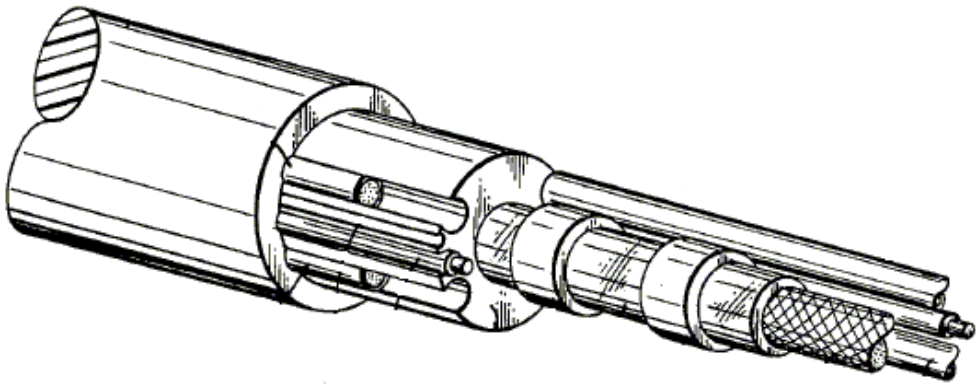

Figure 2.3 VIM model of McGowan and McCulloch [13]

Some inventors realized that ideas from automotive industry could be integrated to this filed. Carpenter and Adkins [14] applied a dash-pot type damper inside VIM. This damper is inserted into cylindrical masses. Movement on visco-elastic core which wraps an elastic strength member causes motion of the masses. Space between masses is filled up with open cell plastic foam. The rest of the inside VIM contains high viscosity fluid. Due to visco-elastic core, dash-pot damper and

masses, VIM provides three different features, namely spring mass isolation, viscous damping and visco-elastic damping (Figure 2.4).

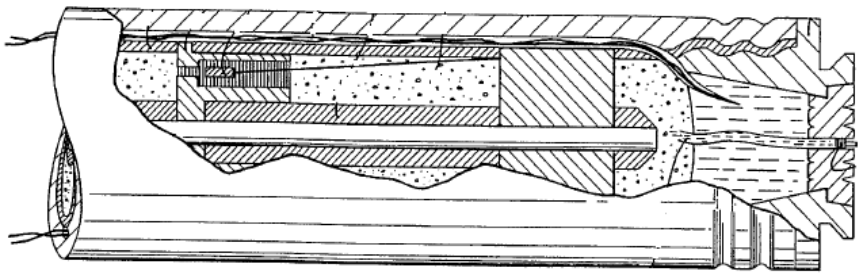

Figure 2.4 Dash-pot damper implementation for VIM [14]

Cameron and Parsons [15] designed a simple VIM structure. Bulkheads and spacer form the skeleton of the VIM. Bulkheads nearly cover the whole cross-section and have high acoustic impedance. In contrast, in order to balance acoustic attenuation, low acoustic impedance spacers are used. They also emphasized on that optimum bulkhead space should be found out to control the desired vibration energy.

Using loss material in VIM can be another alternative solution for vibration isolation. Reynier et al. [16] showed us several types of VIM in which loss materials were utilized. The characteristic of loss material is that there is a certain time difference between stress and strain on material. When a load is applied, deformation will lag with respect to stress. This delay processes adversely, also. When the load is removed, returning to its original shape of the loss material takes time. In the invention, the loss material with ellipsoidal shape is placed into woven sleeve at intervals. These crossly weaved sleeve is connected to both end of the VIM. After some vibrational loads come up on VIM, sleeve tends to become linear so that, loss material inside sleeve will be squeezed and deformed. As an example,

inventors stated a loss angle interval ($0.2 < \tan\delta < 0.5$) for loss material in case of using 10cm diameter VIM. Besides, they expressed that using dash-pot type devices are not suitable due to winding requirement onto winch under load. (Figure 2.5)

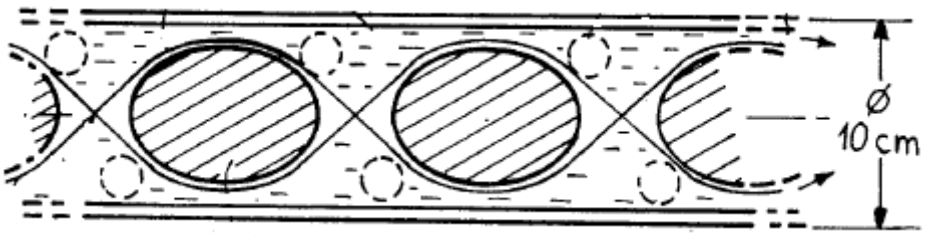

Figure 2.5 One application of using loss material inside VIM [16]

Instead of using elastic or damping properties of core element of VIM with the same direction of load, changing the type of strain might be different approach to vibration isolation solution for towed arrays. Andrews [17] put pitch reversal components onto core cord. Core cord has elastic and damped characteristics. Another cord which is non-extensible was wrapped around core cord helically and attached pitch reversals with the help of pitch reversal clamps. So, longitudinal motion and shocks are converted into torsional strain on elastic core cord due to pitch reversals. Naturally, damping property of VIM comes out as a result of nonlinear interaction between longitudinal and torsional strain. (Figure 2.6)

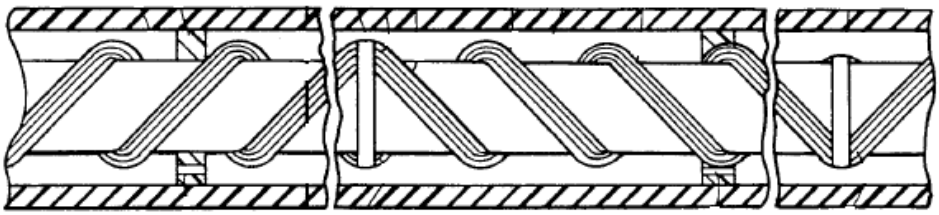

Figure 2.6 VIM design with pitch reversals [17]

As constructed in past, one can produce a basic VIM by using a outer hose, internal fluid and a single elastic rope. However, this rope only resists up to some traction force level and then it will lose its elastic properties. In order to prevent this damaging situation, second elastic rope is added to system. Elastic limits of secondary rope is higher than primary but it is also helpless against excessive drag force. Lastly, third rope which is very strong and non-extensible is provided. First and second rope will work in desired elastic limits and third rope only overcome unexpected load. In the light of this idea, Morningstar and Gill [4] used extensible and non-extensible rope together. Yet, these ropes loop between inner part of transition units and connect the outer part of them instead of lying one end to other of VIM. By playing with the length of the extensible ropes or using different ropes, damping characteristic of VIM can be designated. (Figure 2.7) They patented another VIM design which was quite similar with this one, as well.

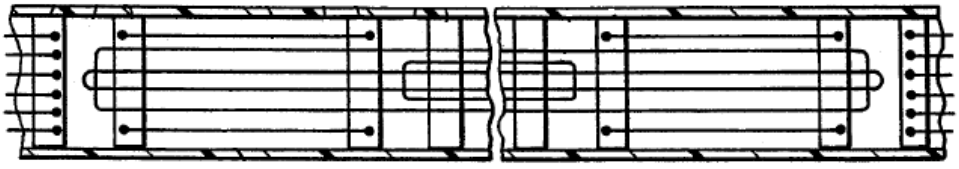

Figure 2.7 VIM design with transition units [4]

VIMs might be become more compact. Harvey`s [18] invention is one of good example for compact VIM structure. Commonly, a core strength member is located at center and non-extensible cords are braided over it along VIM. These two members are enclosed by first inner hose and this hose is filled with gel. Electrical and data cables are placed onto first inner hose then the second inner hose is extruded. Lastly, outer hose is extruded in such a way that wrapping the whole assembly. This type of VIM construction is seemed compact and easy; however, extrusion step at each hosing process would necessitate more attention and be more expensive. (Figure 2.8)

Figure 2.8 More compact VIM assembly [18]

2.2 Studies on Cylindrical Structures Interacting with the Fluid

Until today, many investigations were performed to understand the vibration behavior of cylindrical structures interacting with fluid internally or externally or both. Pipe lines conveying oil, heat exchangers channels and electronic systems towed by vessels inside the sea could be shown as concentrated fields. Why vibration on these structures becomes very important subject is that vibration causes either unexpected structural failures or disturbance on output of the systems. This challenging topic still conserves its topicality. By being utilized developing computer technologies, new methodologies have been improved to estimate the vibration characteristics of fluid coupled cylindrical structures.

In 60`s, it was known that high speed internal flow causes transverse vibration on flexible pipe lines. Paidoussis [19] stated that inertial force of fluid on account of lateral motion of slender structure is common in both axial external flows and internal flows. Because of this, external axial flows set off also vibrational instabilities on slender structures; similarly internal flows. His model for slender structures in axial flow includes classical beam theory modified with inertial force of around fluid due to lateral motion and viscous forces. He conducted an experiment on pinned ends rubber cylinder and compared the results with his model. The results were considerably close and he pointed out that magnitude of axial flow velocity which causes lateral vibrational instabilities is directly proportional with flexural rigidity of structure.

Paidoussis sustained his studies on towed cylinders dynamics and improved stability equations by modifying the frictional force terms [20]. He explained that flexible towed cylinder shows rigid body and flexural instabilities according to towing speeds. He created a different theory for rigid cylinders which possess two degrees of freedom and compared the results with flexible model. For the same shape and boundary conditions, flexural theory and rigid theory give the quite close results for the first two mode frequency.

More comprehensive studies were made on the basis of Paidoussis` works. Experiments, linear and nonlinear dynamic models and comparison of experimental and theoretical results regarding to slender cantilevered cylinder in axial flow were examined in a three-part study. In the first part prepared by Paidoussis et al. [21], new experiments were performed on elastic cylinder in order to clarify dynamic behavior. As stated at previous studies above, it was observed that flow damped the free motion of cylinder at low flow velocities and high flow velocities were required for instabilities. These experiments give also substantially useful information about effects of some geometrical parameters, such as free-end shape, on dynamic behavior. Additionally, energy transfer mechanisms were utilized to predict the physic of instabilities within this study. Lopes et al. [22] stated in the second part of the study that linear model was insufficient to predict

most of the dynamic behaviors. For cantilevered cylinder in axial flow, therefore, they derived nonlinear equation of motion and boundary conditions by means of Hamilton`s principle. Finally, three-part study was concluded by Semler et al. [23]. They utilized finite difference method to solve nonlinear equation derived in the second part and compared theoretical results with experiments performed in the first part. The nonlinear equation of motion was not exact definition of dynamic behavior because nonlinearities of fluid mechanics were not included. However, theoretical results and experiments showed pretty good matches in terms of critical flow velocities, amplitudes and frequencies of instabilities.

Above three-part study might be used to model dynamic behavior of short cylinders in axial flow but solution procedure is defective in solving long cylinders problems. Langre et al. [24] applied another dimensionless analysis for existing linear equation of motion and solved them by using Galerkin method. They focused on flutter problem of cantilever long cylinder, especially effect of length on stability. It was obviously revealed that instabilities occur not through whole structure; they only appears at definite region where is nearby free end. The reason of this situation is decreasing in flow induced tension and it becomes negligible against bending stiffness. Moreover, they evaluated the string model for this kind of case but this model is not acceptable.

Finite element method is one of the solution techniques in stability analysis of towed arrays. Bhattacharyya et al. [25] implemented finite element approximation by using Hamilton`s principle. They verify their approach with some validation and convergence problem. After they showed the reliability of this method, they utilized it to define stability conditions of neutrally buoyant acoustic array with negatively buoyant tow cable at its upstream end.

Acoustic streamer towed behind ships` back is one of the sophisticated examples for fluid-structure interaction problems. Transverse motion of neutrally buoyant section of acoustic array and negatively buoyant section of it were investigated in two-part study by Dowling [2], [26]. She considered the all sections of streamer as

a thin and flexible cylinder. She specified that transverse displacement form of neutral section has not a simple form due to critical point after which tension by fluid drag is ineffective. By using method of match asymptotic expansion and forth-order equation of motion, general solution was formulated. With this study also, forced vibration was examined and attenuation characteristics of flexible cylinder was predicted depending on frequency levels. Furthermore, she reviewed the transverse displacement of cylinder when it was coupled with aft drogue rope. It can be said that using drogue rope is not effective in order to increase attenuation level, especially at high frequencies. The second part of the study concentrated on towing cable which is negatively buoyant and inclined form. Transverse motion of cable was evaluated for horizontal and vertical plane separately. Boundary condition at the downstream of cable was derived from works handled in the first part for neutrally buoyant cylinder. It was stated that towing cable shows distinct attenuation capability for each plane vibrations. This distinction was explained by low-high frequency analytical solution.

Ketchman [10] analyzed the towing cable dynamic vibration problem in order to diminish vibration transmission to the acoustic arrays. Basic string equation with fluid forces was utilized for yaw and pitch transverse vibration. Besides single point excitation, distributed vortex excitation was solved. Also, it was pointed out that, there exist two different longitudinal vibration formations which are direct axial excitations and indirect axial excitations due to transverse vibration. Analytical solutions were performed for longitudinal vibration, as well.

CHAPTER 3

THEORY AND MODELING

In this chapter, some basic concepts which are related with modeling of the VIM structure will be mentioned. Firstly, Timoshenko Beam Theory will be given in shortly. Then, dynamic modulus definition for viscoelastic materials will be explained by utilizing complex number. After that, the most important title, Myklestad-Prohl Method (Myklestad`s Method), is going to be come up. This method is one of the subtitles under the transfer matrix method (TMM) field. Afterwards, modeling of inertial effects within the Myklestad`s Method will be referenced from previous studies. Then, conditions which have to be considered while modeling the VIM will be explained. Finally, Myklestad`s Method will be modified according to these conditions to find out bending natural frequencies of the VIM.

3.1 Theory

3.1.1 Timoshenko Beam Theory

In classical beam theory (Euler-Bernoulli Beam Theory), rotational inertia and angular distortion due to shear are neglected. This theory gives reliable results for only slender beams. However, the situation is a little bit complicated for short and thick beams. Rotation of cross section and deformation due to shear have an importance while defining the short and thick beam`s response. So, addition of rotary inertia and shear effect to classical beam theory was firstly concluded by Timoshenko in 1921 [27]. Timoshenko beam theory gives more accurate results

for beam`s response than Euler-Bernoulli theory when they are compared with results from the exact elasticity equations and experiments [28].

Unlike Euler-Bernoulli beam theory, deflection in y is caused by not only bending but also shear at Timoshenko theory. For very small linear and angular deflections, slope at any x can be written as,

$$\frac{\partial y(x,t)}{\partial x} = \psi(x,t) + \beta(x,t) \tag{3.1}$$

Slope $\psi(x, t)$ is related with bending while $\beta(x, t)$ is related with shear. So, expressions of moment and shear force becomes,

$$M(x,t) = EI\frac{\partial \psi(x,t)}{\partial x} \tag{3.2}$$

$$Q(x,t) = \kappa GA\beta(x,t) \tag{3.3}$$

Take out the $\beta(x, t)$ term from equation (3.1) and substitute it into equation (3.3).

$$Q(x,t) = \kappa GA\left[\frac{\partial y(x,t)}{\partial x} - \psi(x,t)\right] \tag{3.4}$$

According to Figure 3.1, equation of motion of beam element for rotation and transition in y direction can be easily extracted.

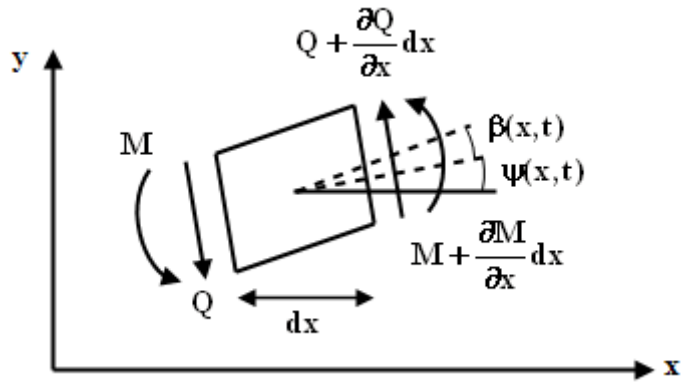

Figure 3.1 Free body diagram of beam element

For transitional motion,

$$Q(x,t)+\frac{\partial Q(x,t)}{\partial x}dx-Q(x,t)=\rho A dx\frac{\partial^2 y(x,t)}{\partial t^2}$$

$$\frac{\partial Q(x,t)}{\partial x}=\rho A\frac{\partial^2 y(x,t)}{\partial t^2} \tag{3.5}$$

Put the equation (3.4) into equation (3.5). New equation becomes,

$$\frac{\partial}{\partial x}\left[\kappa GA\left[\frac{\partial y(x,t)}{\partial x}-\psi(x,t)\right]\right]=\rho A\frac{\partial^2 y(x,t)}{\partial t^2} \tag{3.6}$$

For rotational motion,

$$\left[M(x,t)+\frac{\partial M(x,t)}{\partial x}dx\right]-M(x,t)+\left[Q(x,t)+\frac{\partial Q(x,t)}{\partial x}dx\right]\frac{dx}{2}+Q(x,t)\frac{dx}{2}=\rho I dx\frac{\partial^2\psi(x,t)}{\partial t^2}$$

$$\frac{\partial M(x,t)}{\partial x} + Q(x,t) = \rho I \frac{\partial^2 \psi(x,t)}{\partial t^2} \tag{3.7}$$

Substitute the equation (3.2) and (3.4) into (3.7). Final equation about rotational motion is,

$$\frac{\partial}{\partial x}\left[EI \frac{\partial \psi(x,t)}{\partial x} \right] + \kappa GA\left[\frac{\partial y(x,t)}{\partial x} - \psi(x,t) \right] = \rho I \frac{\partial^2 \psi(x,t)}{\partial t^2} \tag{3.8}$$

Timoshenko beam theory can be represented by equations (3.6) and (3.8). However, eliminating the *ψ(x, t)* term by using these two equations and writing Timoshenko equation as a single equation are also possible. After some rearrangements, Timoshenko beam equation in equation form is expressed as,

$$EI \frac{\partial^4 y}{\partial x^4} - \rho I\left(1 + \frac{E}{\kappa G}\right)\frac{\partial^4 y}{\partial x^2 \partial t^2} + \rho A \frac{\partial^2 y}{\partial t^2} + \frac{\rho^2 I}{\kappa G}\frac{\partial^4 y}{\partial t^4} = 0 \tag{3.9}$$

3.1.2 Viscoelasticity and Dynamic Modulus of Viscoelastic Materials

Usage of viscoelastic materials as engineering materials started long before. Rubbers, foams, thermoplastics and polymers are commonly known viscoelastic materials. Characteristics of this type of materials are to behave like both viscous fluid and elastic solid. Also, behavior of viscoelastic material is defined with three important phenomena which are stress relaxation, creep and hysteresis. Stress relaxation can be explained as decreasing in stress with time when a constant strain is applied to viscoelastic material. Creep has the same analogy with stress relaxation but this property shows change of increasing strain under constant stress. Lastly, dissipation of energy as heat under cyclic load is called hysteresis [29].

Linear viscoelastic theory proposes that there is always a linear proportionality between stress and strain history on viscoelastic material. It must be noted that this

theory is valid only for small deformations and linear materials. Within the boundary of linear viscoelasticity, linear springs and dashpot elements are used in order to compose mathematical models [30].

Maxwell model, Kelvin-Voigt model and standard linear solid (SLS) model are well-known simple rheological models for linear viscoelastic materials. Linear spring and dashpot elements are used for these models. Arrangement of linear spring and dashpot element change model to model. The Maxwell model is represented by a purely elastic spring and a damper in series which is shown in Figure 3.2a. Composition of an elastic spring and a damper in parallel is called as Kelvin-Voigt model in Figure 3.2b. The third model, SLS model, is a little bit enhanced model than other models. As illustrated in Figure 3.2c, Maxwell model with a purely elastic spring in parallel constitute the standard linear solid model.

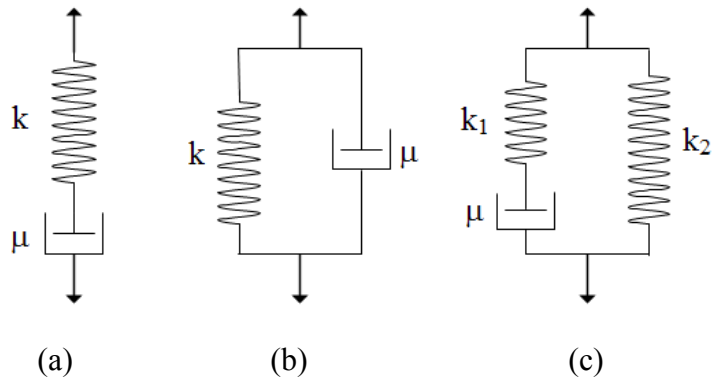

Figure 3.2 Simple rheological models (a) Maxwell Model, (b) Kelvin-Voigt Model, (c) Standard Linear Solid Model (k and μ are elastic and viscous constants)

When the dynamic behavior of viscoelastic materials is examined under cyclic deformation, it is realized that there will be phase difference between strain and stress due to viscoelastic effects. Assume sinusoidal strain which is,

$$\varepsilon(t) = \varepsilon_0 \sin(\omega t) \tag{3.10}$$

where ε_0 and ω are amplitude and angular frequency, respectively. If this strain is applied to pure elastic material, stress will be proportional to strain with the same angular frequency.

$$\sigma(t) = k\varepsilon_0 \sin(\omega t) = \sigma_0 \sin(\omega t) \tag{3.11}$$

Thus, stress is in phase with strain (Figure 3.3a). On the other hand, for purely viscous material, stress can be expressed as,

$$\sigma(t) = \mu \frac{d\varepsilon(t)}{dt} \tag{3.12}$$

Final form of stress due to sinusoidal strain for pure viscous material can be calculated by substituting equation (3.10) into equation (3.12).

$$\sigma(t) = \mu\omega\varepsilon_0 \cos(\omega t) = \sigma_0 \cos(\omega t) = \sigma_0 \sin\left(\omega t + \frac{\pi}{2}\right) \tag{3.13}$$

From equation (3.13), it is obvious that there is a $\pi/2$ phase difference between strain and stress for pure viscous materials (Figure 3.3b). As mentioned before, viscoelastic materials possess both viscous fluid and elastic solid properties. Thus there will be always phase differences, δ, between strain and stress and this value will exist in $(0, \pi/2)$ interval (Figure 3.3c).

$$\sigma(t) = \sigma_0 \sin(\omega t + \delta) \qquad 0 < \delta < \frac{\pi}{2} \tag{3.14}$$

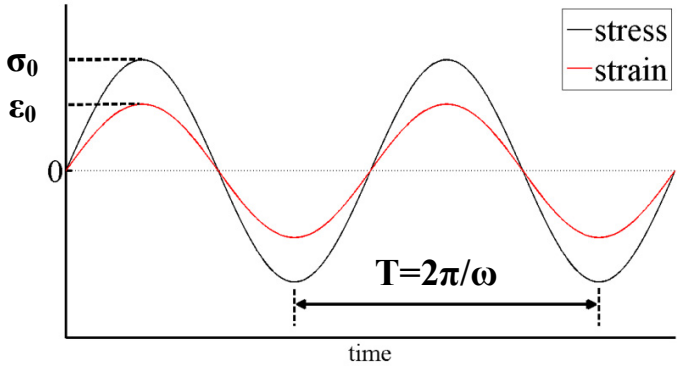

(a)

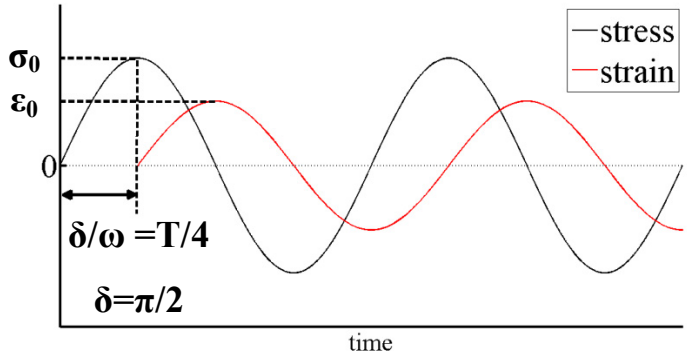

(b)

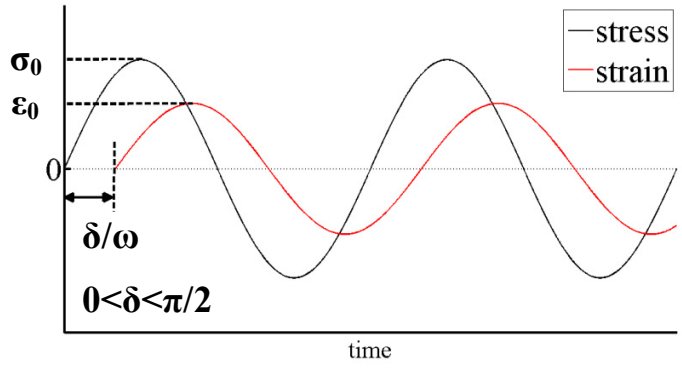

(c)

Figure 3.3 Under cyclic load, stress-strain relation for (a) pure elastic material, (b) pure viscous material and (c) viscoelastic material.

Expression of harmonic functions in complex form is quite convenient for engineering problems. Under cyclic loading, therefore, stress, strain and their relation which is known as *complex dynamic modulus* are expressed in complex for viscoelastic materials. Complex strain and stress of equations (3.10) and (3.14) become,

$$\varepsilon(t) = \varepsilon_0 e^{i\omega t} \tag{3.15}$$

and

$$\sigma(t) = \sigma_0 e^{i(\omega t+\delta)} \tag{3.16}$$

Ratio of the stress to strain gives the complex dynamic modulus, *E**.

$$E^* = \frac{\sigma}{\varepsilon} = \frac{\sigma_0 e^{i(\omega t+\delta)}}{\varepsilon_0 e^{i\omega t}} = \frac{\sigma_0}{\varepsilon_0} e^{i\delta} = \frac{\sigma_0}{\varepsilon_0}(\cos\delta + i\sin\delta) \tag{3.17}$$

Real part of the dynamic modulus is called as *storage modulus* showing stored and recovered energy during periodic load whereas imaginary part is called as *loss modulus* showing dissipated energy due to internal damping. Generally, dynamic modulus is written as,

$$E^* = E_1 + iE_2$$

where

$$E_1 = \frac{\sigma_0}{\varepsilon_0}\cos\delta \quad \textit{and} \quad E_2 = \frac{\sigma_0}{\varepsilon_0}\sin\delta$$

The ratio of imaginary part to real part of dynamic modulus is also important to determine the mechanical properties of viscoelastic materials. This is called as *loss factor*. In other words, loss factor states ratio of lost energy to stored energy. Moreover, loss factor magnitude gives an idea about viscoleastic effect of material. That is, the higher loss factor a material has, the more viscoelastic effect it shows [29].

$$loss\ factor = \tan\delta = \frac{E_2}{E_1} \tag{3.18}$$

Frequency response of dynamic modulus which is extracted by using a simple rheological model varies one model to other. However, these models cannot properly describe the actual dynamic modulus of viscoelastic material. As illustrated in Figure 3.4a, Maxwell model fails at low frequencies due to static stiffness is zero while Kelvin-Voigt model moves away from reality due to infinite loss factor at high frequencies shown in Figure 3.4b. At the same time, standard linear solid model can be used as the basic approach to figure complex modulus out in frequency domain [31].

All of above simple rheological models are effective and quick ways to understand the trend of complex modulus in frequency domain. However, most of the time, they are poor in modeling of viscoelastic properties. That`s why, more complex models were introduced. Generally, these models are in form of combination of basic models. Generalized Maxwell method and generalized Kelvin model can be shown as improved methods.

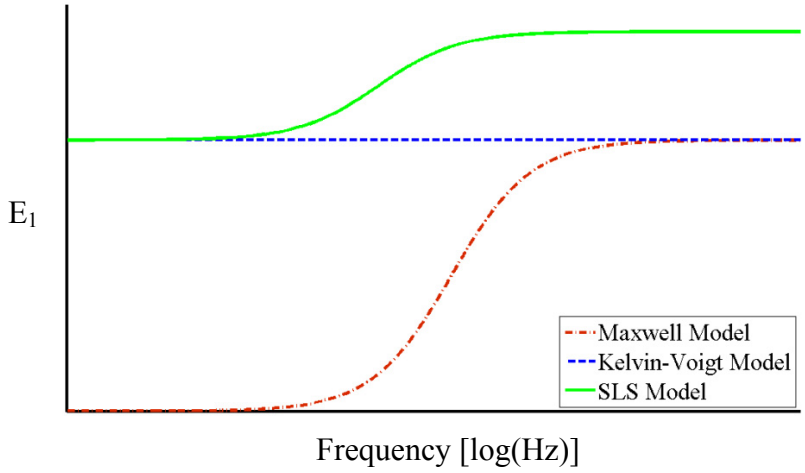

(a)

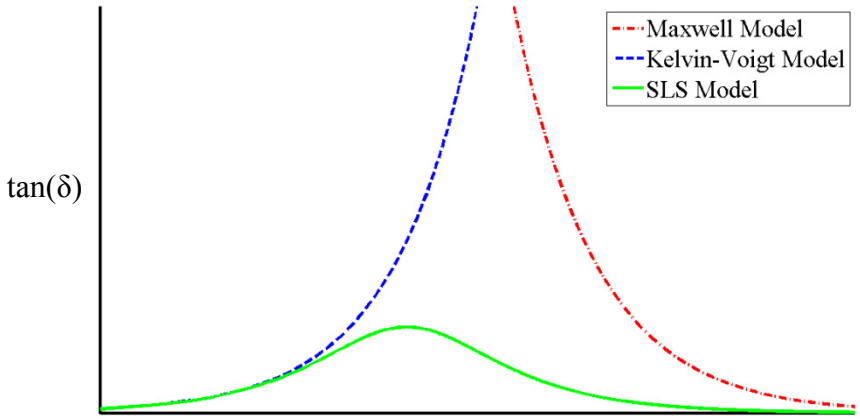

(b)

Figure 3.4 (a) Storage Modulus vs. frequency and (b) loss factor vs. frequency of simple rheological models

3.1.3 Myklestad's - Prohl Method for Bending Vibration

Basically, this method was used to find out the natural frequencies of uncoupled bending vibration of beams which are uniform and have variable stiffness. Although method was developed by Myklestad and Prohl independently, "Myklestad's Method" is the most common name for this method. The origin point of Myklestad's Method is Holzer Method whose field is to solve torsional vibration problems. [32]

Concept of the Myklestad's method is to divide continuous structure, like beam, into segments. The first component of the segment is span; other is called as point mass (Figure 3.5). Span is massless and carry the flexural properties of segment while point mass describe the inertial effects. [33] By constituting field transfer matrixes from spans and point transfer matrixes from point masses, relations between segments are provided. By using these transfer matrixes, overall transfer matrix is written to define one end parameters of structure in terms of other end's. Finally, boundary conditions are put inside the matrix equation and natural frequencies are obtained. However, number of the natural frequencies is limited by number of point masses.

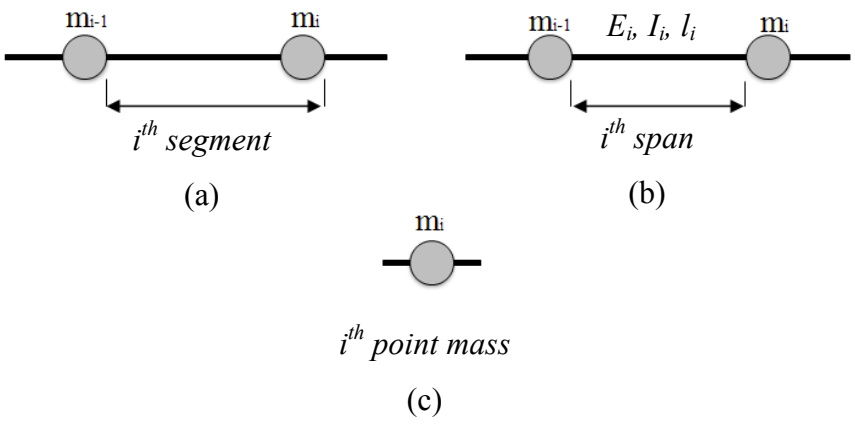

Figure 3.5 (a) Segment, (b) span and (c) point mass section of beam element. [33]

Due to bending of a beam is fourth order, four equations must be written for span and point mass in terms of displacement *(y)*, slope *(ψ)*, shear force *(V)* and moment *(M)*. Also, these four variables constitutes state vector.

Before writing the transfer equations, it is better to define sign convention of four variables. Positive directions can be seen in Figure 3.6.

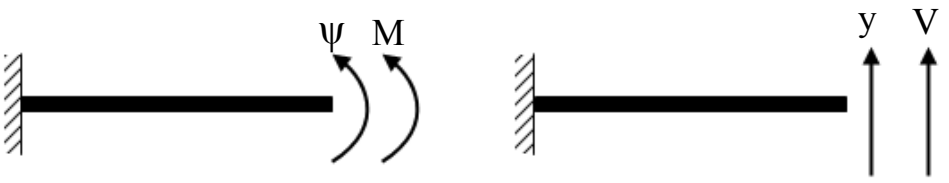

Figure 3.6 Positive sign convention for four variables

In this method, since span is assumed as Euler beam, shear deformations and rotary inertias are not taken into consideration. So, slope at any point of beam is only due to bending. The transfer relation of displacement and slope between ends of the span can be calculated by using general beam deflection formulas.

According to free body diagram in Figure 3.7a, transfer equation of span in terms of shear force and moment are,

$$V_i^L = V_{i-1}^R \tag{3.19}$$

$$M_i^L = M_{i-1}^R - l_i V_i^L \tag{3.20}$$

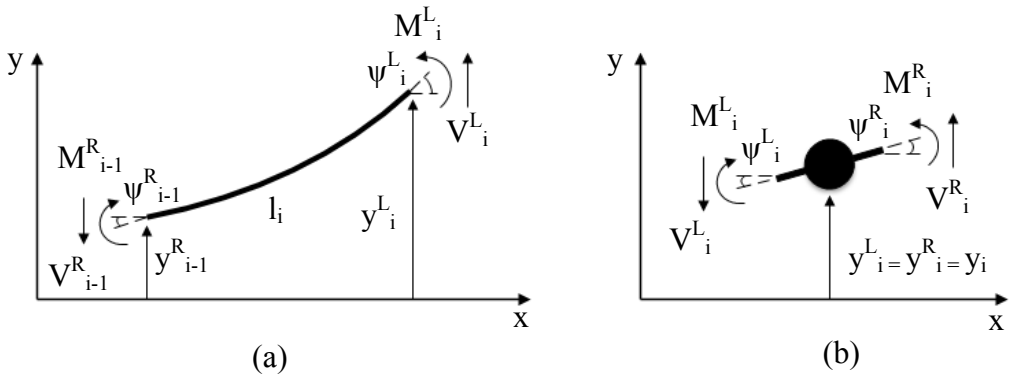

Figure 3.7 Free body diagrams of (a) span and (b) point mass

Superscripts on variables denote the right and left side of i^{th} point mass. Span is considered as a cantilever beam fixed at the left end whereas defining the right end variables. Effects of the slope and displacement at the left end are added to equations. Cantilever beam relations for slope and displacement under both bending moment and shear are [34],

$$\psi = \frac{Ml}{EI} + \frac{Vl^2}{2EI} \tag{3.21}$$

$$y = \frac{Ml^2}{2EI} + \frac{Vl^3}{3EI} \tag{3.22}$$

Slope and deflection equations on span are,

$$\psi_i^L = \psi_{i-1}^R + \frac{M_i^L l_i}{E_i I_i} + \frac{V_i^L l_i^2}{2E_i I_i} \tag{3.23}$$

$$y_i^L = y_{i-1}^R + l_i \psi_{i-1}^R + \frac{M_i^L l_i^2}{2E_i I_i} + \frac{V_i^L l_i^3}{3E_i I_i} \tag{3.24}$$

Let's write down the right end variables as the combination of the left end variables. Firstly, put the equation (3.19) into (3.20). So,

$$M_i^L = M_{i-1}^R - l_i V_{i-1}^R \tag{3.25}$$

Write the equations (3.19) and (3.25) into equation (3.23),

$$\psi_i^L = \psi_{i-1}^R + \frac{\left(M_{i-1}^R - l_i V_{i-1}^R\right) l_i}{E_i I_i} + \frac{V_{i-1}^R l_i^2}{2E_i I_i} \tag{3.26}$$

Rearrange above equation,

$$\psi_i^L = \psi_{i-1}^R + \frac{M_{i-1}^R l_i}{E_i I_i} - \frac{V_{i-1}^R l_i^2}{2E_i I_i} \tag{3.27}$$

This time, put the equations (3.19) and (3.25) into equation (3.24)

$$y_i^L = y_{i-1}^R + l_i \psi_{i-1}^R + \frac{\left(M_{i-1}^R - l_i V_{i-1}^R\right) l_i^2}{2E_i I_i} + \frac{V_{i-1}^R l_i^3}{3E_i I_i} \tag{3.28}$$

Equation finally becomes,

$$y_i^L = y_{i-1}^R + l_i \psi_{i-1}^R + \frac{M_{i-1}^R l_i^2}{2E_i I_i} - \frac{V_{i-1}^R l_i^3}{6E_i I_i} \tag{3.29}$$

By using equations (3.19), (3.25), (3.27) and (3.29), field transfer matrix will be,

$$\begin{bmatrix} y \\ \psi \\ M \\ V \end{bmatrix}_i^L = \begin{bmatrix} 1 & l & \frac{l^2}{2EI} & -\frac{l^3}{6EI} \\ 0 & 1 & \frac{l}{EI} & -\frac{l^2}{2EI} \\ 0 & 0 & 1 & -l \\ 0 & 0 & 0 & 1 \end{bmatrix}_i \begin{bmatrix} y \\ \psi \\ M \\ V \end{bmatrix}_{i-1}^R \tag{3.30}$$

In closed form, field transfer matrix equation is,

$$[S]_i^L = [F]_i [S]_{i-1}^R \tag{3.31}$$

where *[S]* is state vector and *[F]* is field transfer matrix.

According to free body diagram shown in Figure 3.7b, equations of state vector variables are calculated as fallows.

$$y_i^R = y_i^L \tag{3.32}$$

$$\psi_i^R = \psi_i^L \tag{3.33}$$

$$M_i^R = M_i^L \tag{3.34}$$

From dynamic equilibrium

$$V_i^R = V_i^L + m_i \ddot{y}_i \tag{3.35}$$

Since it is a free vibration problem, y_i is assumed as harmonic, $y_i = A_i e^{i(\omega t - \phi)}$. Thus acceleration can be expressed as $\ddot{y}_i = -\omega^2 y_i$. After put the new form of acceleration into equation (3.35), we get,

$$V_i^R = V_i^L - \omega^2 m_i y_i \tag{3.36}$$

Point transfer matrix can be written as,

$$\begin{bmatrix} y \\ \psi \\ M \\ V \end{bmatrix}_i^R = \begin{bmatrix} 1 & 0 & 0 & 0 \\ 0 & 1 & 0 & 0 \\ 0 & 0 & 1 & 0 \\ -\omega^2 m & 0 & 0 & 1 \end{bmatrix}_i \begin{bmatrix} y \\ \psi \\ M \\ V \end{bmatrix}_i^L \tag{3.37}$$

In shortly,

$$[S]_i^R = [P]_i [S]_i^L \tag{3.38}$$

where *[P]* is the point transfer matrix. After substituting the equation (3.31) into equation (3.38), we have,

$$[S]_i^R = [P]_i [F]_i [S]_{i-1}^R \tag{3.39}$$

If we rewrite the above equation in a simple form

$$[S]_i^R = [T]_i [S]_{i-1}^R \tag{3.40}$$

[T] can be called as transfer matrix for segment.

As a result, relations between segments can be found by using equations (3.31) and (3.38) basically. Multiplication of related field transfer matrixes and point transfer matrixes make up the overall transfer matrix. This overall matrix indicated by *[U]* can be seen in following example.

$$[S]_n^R = [U][S]_0^R \tag{3.41}$$

Way of the finding natural frequencies is to apply boundary conditions in equation (3.41). Boundary conditions of both ends are implemented in state vectors. The ω value or values which are meet the all boundary conditions at the ends are calculated with basic matrix operations.

3.2 Equivalent Point Mass and Rotary Inertia for Segments

Generally, lumped masses are located at the middle of the each division in discretization process. Total value of this mass is calculated by summing the half value of adjacent spans. Wu and Chen [35] discretized mass and rotary inertia of the Timoshenko beam on which concentrated elements with eccentricity are exist by using this approach. Also, in the solution of solid prismatic bar free vibration by Sule [36], lumped masses are calculated from half values of near spans. Some methods used to determine normal modes and natural frequencies of torsional and flexural vibrations were collected in Minhinnick`s [37] study. He also indicated using concentrated mass at the gravity center of span in Myklestad`s method. To be able to solve eigenvalues of rotor-bearing systems faster, Al-Bahkali and ElMadany [38] developed a code based on transfer matrix. All inertial effects of span are turned into point mass properties at the end of the span. In case of interested beam or shaft is not uniform cross section, again point mass inertial properties constitute of half of next spans. Darlow et al. [39] calculated each half span property for conical shaft individually instead of writing the all span inertial property as a lumped mass. However, apart from general approach, new method to define point mass inertial effects was implemented by Nakano [40]. Total properties were separated into two parts and located at the each end of span. Magnitudes of these parts are proportional to distances which are from end to mass center of span.

In this thesis, general approach which is proved at previous works above will be utilized. Inertial properties of span will be described by using neighbor spans and put the mass center of the span. Even though Darlow et al. and Nakano proposed

new techniques on calculating equivalent mass and equivalent rotary inertia, they give the same results with general approach for uniform beams or shafts.

3.3 Mathematical Model of the VIM

Thinking of drag force in the sea water, the hung VIM model will be more reasonable approach for modeling. Because of the fact that tension on VIM structure as a result of drag shows horizontal distance dependency. In short, tension magnitude at any section is directly proportional to length of the structure which remains behind that section. So, gravitational force has the same characteristic with drag force. Tension increases while being moved upward. However, since this model is the introduction step to figure VIM dynamic out, damping effect or other effects of sea water around structure during tow action are not taken into consideration in this study.

Spacers are placed inside the hose with a nominal gap value. Since the outer surfaces of the spacers tightly contact with the inner surface of the hose, they divide the VIM into many identical and repeating sub-structures. Physical properties of them are almost the same. From this perspective, it was considered that each portion between spacers behaves as a span and each spacer behaves as a point mass. Thus, Myklestad`s Method seems a convenient way to understand the dynamics of the VIM structure. However, basic equation of this method in section 3.1.3 does not describe the hung VIM properly. First of all, all formulations were derived from Euler beam theory in classical Myklestad`s Method. In other words, shear deformation was neglected and only slope due to rotation was taken into consideration. Moreover, rotary inertias are also neglected. But in the VIM structure, length to thickness ratio of span is very small to use Euler beam theory so; shear deformation will have an important influence on our system dynamic.

Since the hung VIM is subjected to gravity, tension on spans and point masses exists, as in Figure 3.8. It is required that adding this variable tension to the system modeling.

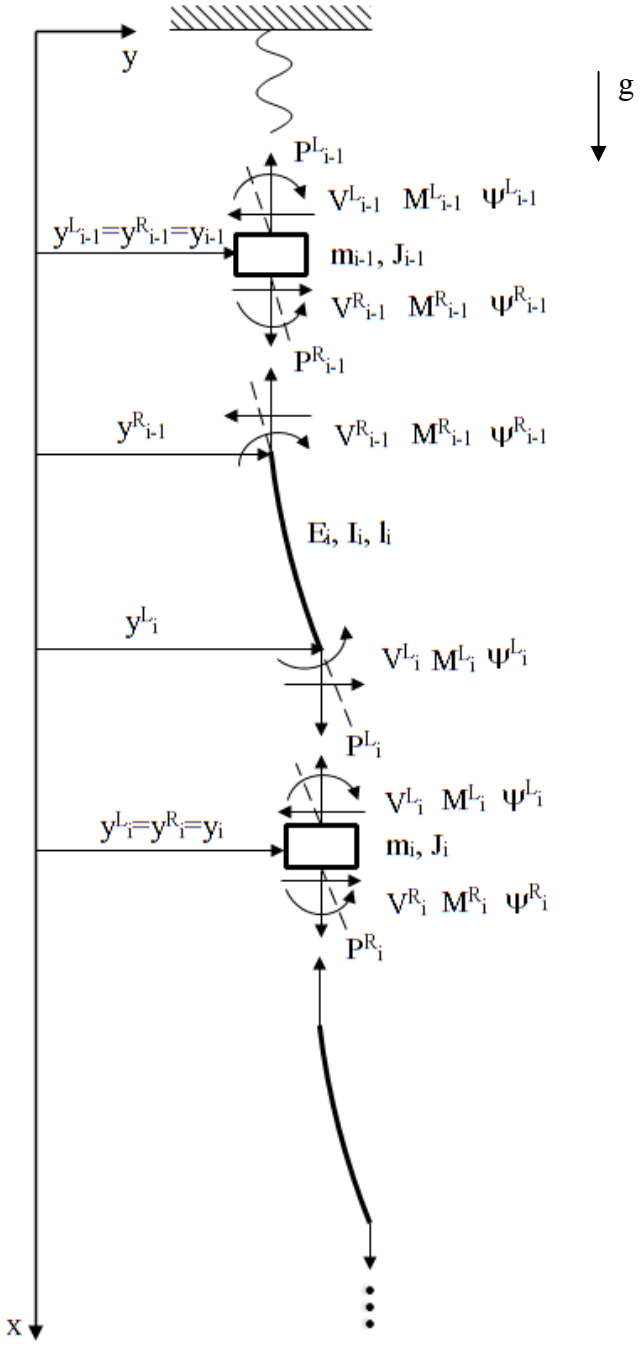

Figure 3.8 Discretized model of the hung VIM

In modeling, elastic properties such as elastic modulus and shear modulus would be in complex form resulting from hose of the VIM, i.e., span because the hose is

made of viscoelastic material. Chen and Ding [41], in their study, investigated how properties of viscoelastic beam affect the steady state response of beam under transverse load. While writing the axial stress distribution, they utilized the Kelvin model to state the relation between stress and strain. If stress and strain is assumed as harmonic in this formula, elastic modulus will concluded as complex quantity. For lateral vibration again, West [42] also included viscoelastic properties of beam by using both complex elastic modulus and shear modulus. Viscoelastic materials shows phase difference between input and output response according to Ikegami [43]. He explained that complex elastic properties can be used to define viscoelastic effects.

The VIM is filled with an incompressible fluid, izopar that is petroleum extended oil. Due to this fluid is filled under pressure, there is no void inside. By draining the excessive amount of liquid, inside pressure of VIM is balanced with atmospheric pressure. That's why fluid would not move inside hose relatively. So, it is assumed that fluid inside the VIM does not create viscous damping effect for dynamic of system. In defining response of a fluid conveying pipe under vertical earthquake excitation, internal damping effects of fluid are neglected by Petkova and Kisliakov [44]. If the fluid velocity exists, some momentum terms and only mass are added to solution in terms of fluid side. Wiggert and Tijsseling [45] investigated on fluid-structure interaction in piping system. Three vibration types; axial, lateral and torsional, are considered uncoupled each other. Used model for piping system lateral vibration includes fluid as added mass. As a result, thinking the effect of izopar inside VIM as added mass becomes convenient approach.

To sum up, extended Myklestad`s Method which would be modified according to Timoshenko beam theory concepts will be utilized for the hung VIM model. Shear deformation and rotary inertia with axial load would have been implemented into classical Myklestad`s Method at the same time. Viscoelastic characteristic of the VIM hose will be handled with complex elastic modulus. Lastly, other than added mass and rotary inertia effect, all effects of the internal fluid (izopar) would be neglected.

3.4 Modified Myklestad`s Method for the Hung VIM

There are two new parameters effecting the equations for field transfer matrix. The first one is axial force due to gravity, other one is shear deformation. Related with first one, Wei et al. [46] add the gravitational force on each span as axial force while analyzing the natural frequencies of wind turbine tower. Spans which are at bottom are exposed to more axial force than upper spans. Due to spans are assumed massless, axial force through span is constant thus, coupled moment occurs.

Shear deformation rotary inertia was included in Myklestad`s Method before. Wu and Chen [35] attained a satisfactory model for multi-step Timoshenko beam carrying eccentric lumped masses. This extended method gives substantially consistent results with conventional methods like FEM. Moreover, Myklestad`s Method strongly stands out in rotor dynamic field. As a special case, conical section beams was investigated with this method by Darlow et al. [39]. Shear deformation effect can be noticed inside the field matrix obviously.

Free body diagrams of span and point mass including axial force can be seen in Figure 3.9. Axial force is assumed acting only x-axis so that shear force equation of modified model would be the same with Equation (3.19).

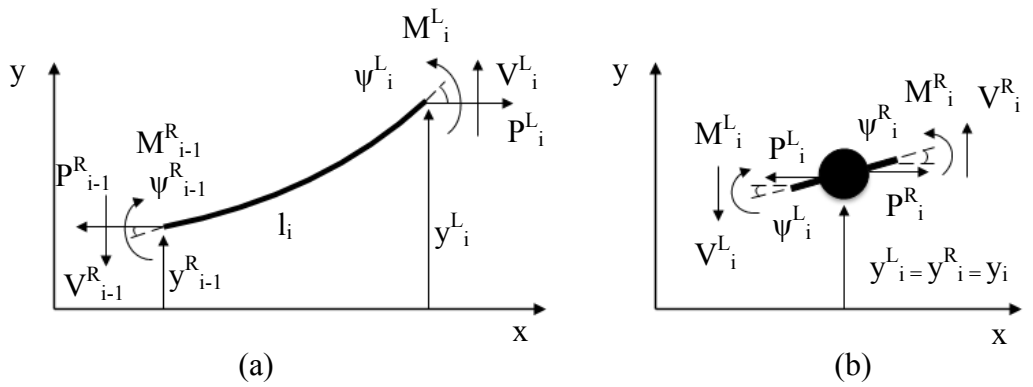

Figure 3.9 Free body diagram with axial force of (a) span and (b) point mass

Tensions occurred on segment ends were due to weight of the spans. Axial force through each span is taken as constant in modified method because segment is assumed as massless. Tension on any segment may be equal to zero, only its weight or sum of many segment weights. For instance, this tension force is zero at the bottom end of the VIM and magnitude of this force is calculated at any segment by summing the weight of other segments which stands under interested point. Thus, variable tension force on the VIM is expressed with many constant tension forces on segments. The number of these discrete tension forces is as much as the number of segments.

$$P_{i-1}^{R} = P_{i}^{L} = P_{i} \tag{3.42}$$

$$P_{i} = \sum_{k=i}^{N} m_{k} g \tag{3.43}$$

where N denotes total number of masses. As mentioned before, equal axial force creates couple moment and forces at ends cancel each other. Moment equation on span becomes,

$$M_{i}^{L} = M_{i-1}^{R} - l_{i} V_{i}^{L} + P_{i}(\mathrm{y}_{i}^{L} - \mathrm{y}_{i-1}^{R}) \tag{3.44}$$

It must be noted while writing slope equation that only slope from bending (rotation) should be taken into consideration. Basic equation is,

$$\frac{d\psi}{dx} = \frac{M}{EI} \tag{3.45}$$

As shown in Figure 3.10, total bending moment at any section on beam results as,

$$M_{total} = M - P\left(y_{l} - y_{0}\right) + V\left(l - x\right) \tag{3.46}$$

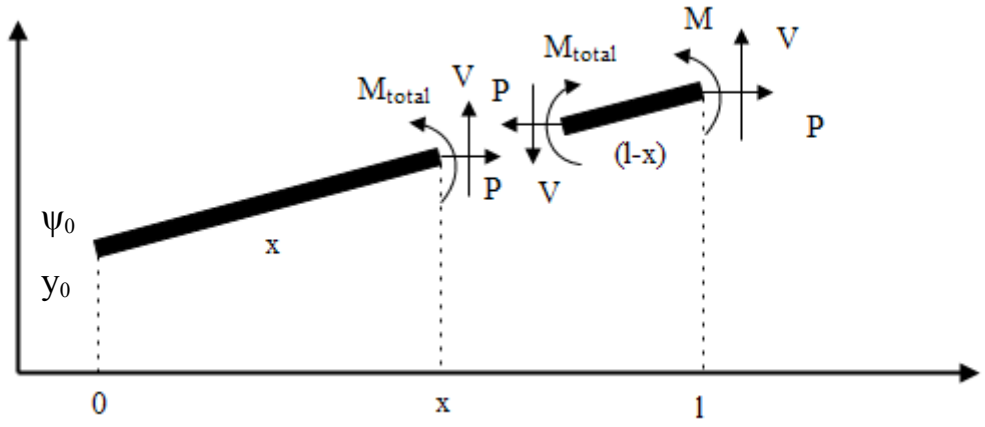

Figure 3.10 Moment equation at any section

Substitute the equation (3.46) into equation (3.45) and take integral,

$$d\psi = \frac{1}{EI}\left[M - P\left(y_l - y_0\right) + V\left(l - x\right)\right]dx$$

$$\int d\psi = \frac{1}{EI}\int\left[M - P\left(y_l - y_0\right) + V\left(l - x\right)\right]dx$$

$$\psi\left(x\right) = \frac{Mx}{EI} + \frac{Vx\left(2l - x\right)}{2EI} - \frac{P\left(y_l - y_0\right)}{EI} + C_1 \qquad (3.47)$$

By applying boundary conditions at x=0, constant C_1 will be equal to slope of left end. Final slope equation depending on x becomes,

$$\psi\left(0\right) = C_1 = \psi_0 \qquad at\ x = 0$$

$$\psi\left(x\right) = \psi_0 + \frac{Mx}{EI} + \frac{Vx\left(2l - x\right)}{2EI} - \frac{Px\left(y_l - y_0\right)}{EI} \qquad (3.48)$$

For field matrix, slope equation of span seen in Figure 3.9a can be arranged according to above equation.

$$\psi_i^L = \psi_{i-1}^R + \frac{M_i^L l_i}{E_i I_i} + \frac{V_i^L l_i^2}{2E_i I_i} - \frac{P_i l_i \left(y_i^L - y_{i-1}^R\right)}{E_i I_i} \tag{3.49}$$

Displacement relation between ends shows difference than classical equations because shear deformation increases the lateral deflection as well. With Euler beam theory this effect is neglected but Timoshenko beam theory is not.

$$\frac{dy}{dx} = \psi + \beta \tag{3.50}$$

$$\beta = \frac{V}{\kappa AG} \tag{3.51}$$

where β is slope due to distortion and κ is shear coefficient. In order to extract displacement relation, put the equations (3.48) and (3.51) into (3.50) and take integral.

$$dy = \left[\left[\psi_0 + \frac{Mx}{EI} + \frac{Vx\left(2l - x\right)}{2EI} - \frac{Px\left(y_l - y_0\right)}{EI}\right] + \frac{V}{\kappa AG}\right]dx$$

$$\int dy = \int\left[\psi_0 + \frac{Mx}{EI} + \frac{Vx\left(2l - x\right)}{2EI} - \frac{Px\left(y_l - y_0\right)}{EI} + \frac{V}{\kappa AG}\right]dx$$

$$y(\mathrm{x}) = \psi_0 x + \frac{Mx^2}{2EI} + \frac{Vx^2\left(3l - x\right)}{6EI} - \frac{Px^2\left(y_l - y_0\right)}{2EI} + \frac{Vx}{\kappa AG} + C_2 \tag{3.52}$$

Again using boundary condition at x=0, constant C_2 and displacement equation are,

$$y(0) = C_2 = y_0 \qquad at\ x = 0$$

$$y(\mathrm{x}) = y_0 + \psi_0 x + \frac{Vx}{\kappa AG} + \frac{Mx^2}{2EI} + \frac{Vx^2\left(3l - x\right)}{6EI} - \frac{Px^2\left(y_l - y_0\right)}{2EI} \tag{3.53}$$

Modified displacement equation for span with shear displacement and axial force can be found clearly from equation (3.53)

$$y_i^L = y_{i-1}^R + \psi_{i-1}^R l_i + \frac{V_i^L l_i}{\kappa A_i G_i} + \frac{M_i^L l_i^2}{2E_i I_i} + \frac{V_i^L l_i^3}{3E_i I_i} - \frac{P_i l_i^2\left(y_i^L - y_{i-1}^R\right)}{2E_i I_i} \tag{3.54}$$

Transfer matrix is generally composes between right state variables and left state variables. Thus, all variables right span end should be written in terms of left span end variables. Substitute the equations (3.19) and (3.44) into (3.49) and arrange,

$$\psi_i^L = \psi_{i-1}^R + \frac{\left(M_{i-1}^R - l_i V_i^L + P_i(\mathrm{y}_i^L - \mathrm{y}_{i-1}^R)\right) l_i}{E_i I_i} + \frac{V_i^L l_i^2}{2E_i I_i} - \frac{P_i l_i\left(y_i^L - y_{i-1}^R\right)}{E_i I_i}$$

$$\psi_i^L = \psi_{i-1}^R + \frac{M_{i-1}^R l_i}{E_i I_i} - \frac{V_{i-1}^R l_i^2}{2E_i I_i} \tag{3.55}$$

Finding displacement equation is quite similar with slope equation. As a result of combination of equations (3.19), (3.44) and (3.54),

$$y_i^L = y_{i-1}^R + \psi_{i-1}^R l_i + \frac{V_{i-1}^R l_i}{\kappa A_i G_i} + \frac{\left(M_{i-1}^R - l_i V_i^L + P_i(\mathrm{y}_i^L - \mathrm{y}_{i-1}^R)\right) l_i^2}{2E_i I_i} + \frac{V_i^L l_i^3}{3E_i I_i} - \frac{P_i l_i^2\left(y_i^L - y_{i-1}^R\right)}{2E_i I_i}$$

$$y_i^L = y_{i-1}^R + \psi_{i-1}^R l_i + \left(\frac{l_i}{\kappa A_i G_i} - \frac{l_i^3}{6E_i I_i} \right) V_{i-1}^R + \frac{M_{i-1}^R l_i^2}{2E_i I_i} \tag{3.56}$$

Now, put the equation (3.56) adversely into (3.44)

$$M_i^L = M_{i-1}^R - l_i V_i^L + P_i(\psi_{i-1}^R l_i + \frac{V_{i-1}^R l_i}{\kappa A_i G_i} + \frac{M_{i-1}^R l_i^2}{2E_i I_i} - \frac{V_{i-1}^R l_i^3}{6E_i I_i})$$

$$M_i^L = \left(1 + \frac{P_i l_i^2}{2E_i I_i}\right) M_{i-1}^R + \left(\frac{P_i l_i}{\kappa A_i G_i} - \frac{P_i l_i^3}{6E_i I_i} - l_i \right) V_{i-1}^R + \psi_{i-1}^R l_i P_i \tag{3.57}$$

All equations required for transfer matrix field of the VIM span is extracted. There has been no change in shear force equation. Moment equation includes axial force component intensely. Slope equation have not been affected neither shear deformation nor axial force. Lastly, shear deformation term is added into deformation equation as being outcome of Timoshenko beam assumption.

Let's write down the field transfer matrix of VIM model.

$$\begin{bmatrix} y \\ \psi \\ M \\ V \end{bmatrix}_i^L = \begin{bmatrix} 1 & l & \frac{l^2}{2EI} & \left(\frac{l}{\kappa AG} - \frac{l^3}{6EI} \right) \\ 0 & 1 & \frac{l}{EI} & -\frac{l^2}{2EI} \\ 0 & lP & \left(1 + \frac{Pl^2}{2EI}\right) & \left(\frac{Pl}{\kappa AG} - \frac{Pl^3}{6EI} - l \right) \\ 0 & 0 & 0 & 1 \end{bmatrix}_i \begin{bmatrix} y \\ \psi \\ M \\ V \end{bmatrix}_{i-1}^R \tag{3.58}$$

Compact form of above equation can be defined similarly with equation (3.31). Adding rotary inertia is another modification on basic method. From Figure 3.9b, moment equilibrium including rotary inertia is,

$$M_i^R = M_i^L + J_i \ddot{\psi}_i \tag{3.59}$$

For free vibration case, harmonic motion expression can be appropriately used for slope. Final state of above equation is arranged as,

$$\psi_i = \Psi e^{i(\omega t - \delta)}$$

$$\ddot{\psi}_i = -\omega^2 \psi_i$$

$$M_i^R = M_i^L - \omega^2 J_i \psi_i \tag{3.60}$$

By using the equations from section 3.1.3, point transfer matrix can be written as follow.

$$\begin{bmatrix} y \\ \psi \\ M \\ V \end{bmatrix}^R = \begin{bmatrix} 1 & 0 & 0 & 0 \\ 0 & 1 & 0 & 0 \\ 0 & -\omega^2 J & 1 & 0 \\ -\omega^2 m & 0 & 0 & 1 \end{bmatrix}_i \begin{bmatrix} y \\ \psi \\ M \\ V \end{bmatrix}_i^L \tag{3.61}$$

Modifications can be easily seen from field transfer matrix and point transfer matrix of hanged VIM model. At the beginning, shear deformation effects and rotary inertia in point transfer matrix exist inherently as a result of Timoshenko beam theory. Additionally, gravitational force is considered only acting on x-axis, taken into account as coupled moment on span.

CHAPTER 4

EXPERIMENTAL STUDIES

In this chapter, experimental work on a VIM sample will be described. Modal impact testing technique has been applied during experiment. Firstly, general information about this technique will be given. Then, test setup will be explained. Finally, test results of the VIM sample will be given.

4.1 Modal Impact Test

Modal test is a common method of determining modal parameters which are resonance frequencies, mode shapes and damping values of the structure. In this method, test structure is excited with a force whose frequency content is known and response of the structure is measured. Then, transfer function which is called frequency response function (FRF) is obtained by using both force spectra and response spectra. This function actually defines response per unit force. According to type of response, FRF is represented in different ways. Well-known FRF types are accelerance, mobility and compliance respectively. The ratio of the acceleration response spectrum to force spectrum gives accelerance. Mobility represents the ratio of the velocity response spectrum to force spectrum. Lastly, the ratio of the displacement response spectrum to force spectrum defines receptance. Although these functions are apart from each other, they provide the same information about modal parameters. The FRF is generally expressed in curve fitted form and modal parameters can be easily extracted.

During evaluation of the test results, three important assumptions related with test structure must be made. The first one is that the structure is assumed to show

linear behavior. The second is that parameters of the structure are assumed to not vary with time, namely, time-invariant. The last one is that the structure is assumed to obey Maxwell`s reciprocity. Without these assumptions, modal test and analysis will be meaningless.

Today, modal test can be performed in many ways. Modal impact test is the popular one. The history of the impact test began at 1970`s with the developing FFT (Fast Fourier Transform) analyzers [47]. Advantages of the modal impact test are to be fast, convenient and inexpensive but this test method is not appropriate for nonlinear structures. Typical equipments of the modal impact test are an impact hammer, accelerometer, minimum 2 or 4 channel (depending on axes of accelerometer) FFT analyzer and post-processor center (Figure 4.1). Impact hammer is used to excite the structure in a broadband. Input force is measured by means of a load cell which is attached to tip of the hammer. To be able to supply sufficient energy to the structure, size of the hammer should be selected properly. Additionally, tip hardness of the hammer should be defined according to frequency of interest. Hard tips create short pulse and cover the wide frequency range whereas soft tips create long pulse and cover narrow frequency range. Accelerometer measures the response in terms of acceleration. FFT analyzer computes the FRFs and modal parameters are identified by post-processing center.

Modal impact test steps can be given in following order. Firstly, the structure is exited by impact hammer and force data is sent to FFT analyzer. Then, response of the structure is measured by accelerometer and the output is sent to FFT analyzer as well as force data. After that, FRF is computed from these force and response data by FFT analyzer. Finally, post- processing center defines the modal parameters and makes them visual.

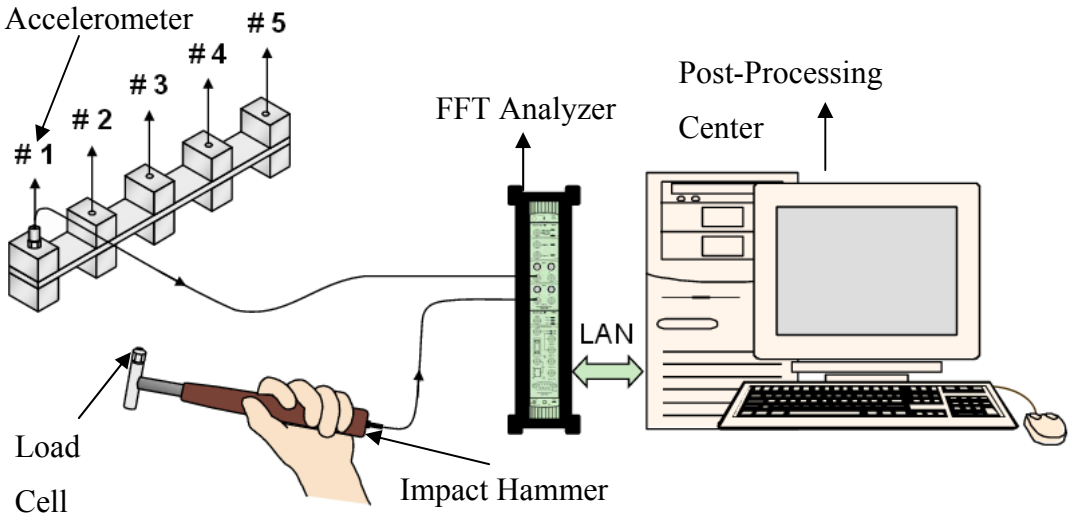

Figure 4.1 Typical setup for modal impact test

It must be noted that only global parameters which are resonance frequencies and damping values can be acquired from a single FRF. This means that, one accelerometer and one impact hammer are sufficient for determination of the global properties. However, more than one FRF are needed to estimate the mode shapes accurately. One should be extremely careful while determining the number of FRFs not to miss out mode shapes. FRFs are expressed in matrix form and both response and input force in vector form. Thus, at least one column or one row of the FRF matrix must be known for mode shape identification. To be able to find out either all row elements or column elements of FRF matrix, there exist three different modal impact test implementation. These are single input multiple output (SIMO) modal impact test, multiple input single output (MISO) modal impact test and multiple input multiple output (MIMO) modal impact test. Following sections will mention about these implementations in brief.

4.1.1 Single Input Multiple Output (SIMO) Impact Test

The input force is applied to a single point on the structure. Response data are collected from many locations. As a result, a full column of FRF matrix has been obtained. Demonstration of the SIMO impact test and resultant FRF matrix are given in Figure 4.2 and Figure 4.3 respectively. The remarkable point about multiple output impact tests is that they make data consistency optimization possible.

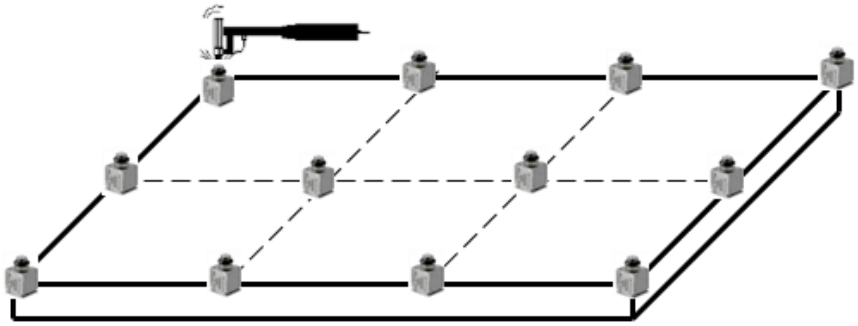

Figure 4.2 Single input multiple output (SIMO) impact test

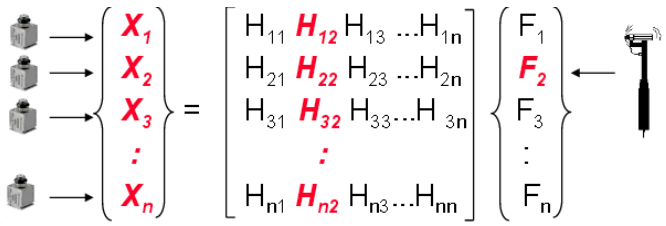

Figure 4.3 FRF matrix of single input multiple output impact test

4.1.2 Multiple Input Single Output (MISO) Impact Test

In this method, input force is applied to many different points and response is only measured from a single reference point. So, one row of the FRF matrix is defined. Because of FRF matrix is symmetric, a column can be extracted by utilizing defined row so that mode shapes can be easily determined. Multiple input single output impact test is shown in Figure 4.4 and related FRF matrix is given in Figure 4.5.

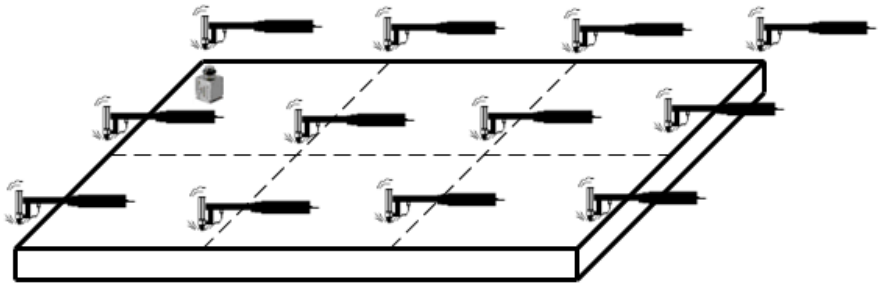

Figure 4.4 Multiple input single output (MISO) impact test

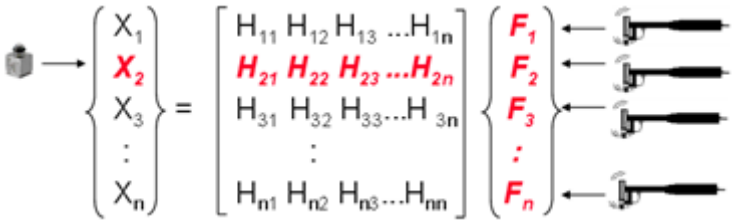

Figure 4.5 FRF matrix of multiple input single output impact test

4.1.3 Multiple Input Multiple Output (MIMO) Impact Test

Test is performed by exciting the system at more than one location and collecting the response data from again many points on the structure. At the end, more than one column or row of FRF matrix can be calculated as depending on number of output and input. Figure 4.6 and Figure 4.7 show the test technique and FRF matrix respectively.

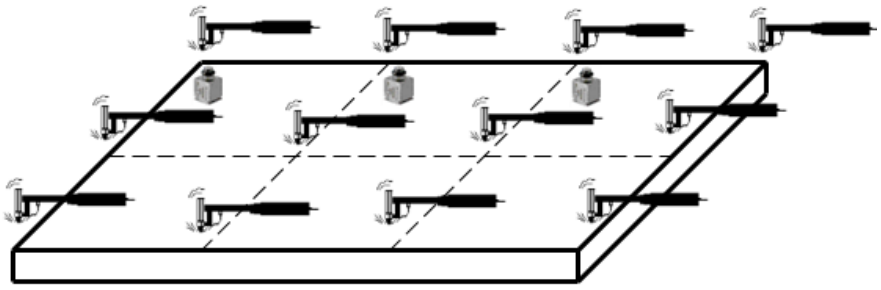

Figure 4.6 Multiple input multiple output (MIMO) impact test

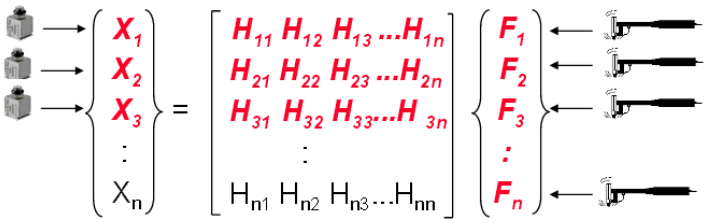

Figure 4.7 FRF matrix of multiple input multiple output impact test

In some cases, single row or column FRFs cannot be adequate to get all modal information about the structure. One of them is having repeated roots, i.e., identical modes will occur at different planes when the structure is symmetric. So, both excitation number and response number must be at least two. Other situation necessitating more column or row is having local modes. This means that, number available force inputs fall short to excite all modes. It should be noted that it is also possible to complete full FRF matrix with this test method.

4.2 Experimental Setup

Experimental studies were performed on a VIM to verify modified Myklestad`s Method. A SIMO modal impact tests were performed for the VIM. As mentioned before, VIMs work in the water and a variable drag force on them occur during towing action. That's why; the method in Chapter 3 was expanded by inserting variable tension force. It was thought that the hung VIM would be a proper implementation to simulate this drag force. Sample VIM was hanged to the overhead winch frame with a slim rope (Figure 4.8). Thus, free-free boundary conditions were almost satisfied.

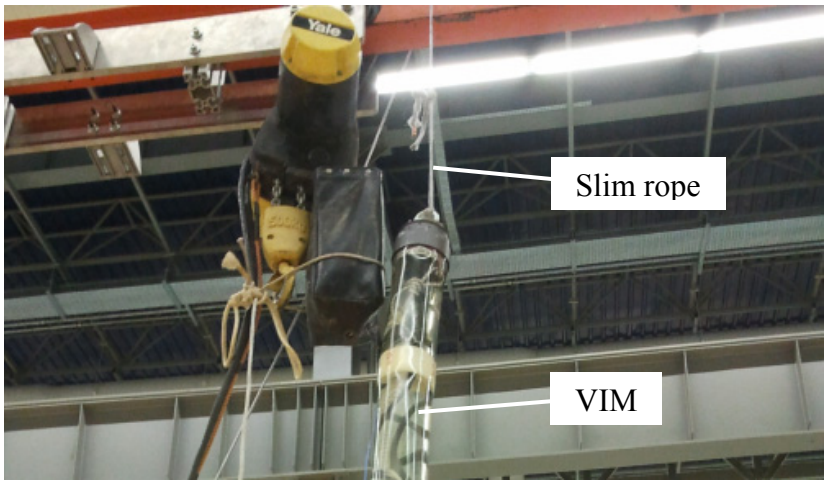

Figure 4.8 Application of hanged VIM

First of all, the VIM sample was prepared to check the reliability of developed method. The sample was classical type VIM. It had a length of 2.79m and spacers were placed with a distance of 22cm.

VIM hoses are thermoplastic polyurethane base materials. Because of their nature, they show viscoelastic behavior. This means that effects of the structural damping cannot be ignored. Unlike metals, modulus of elasticity value would be in complex form designating storage and loss modulus together. Moreover, elastic properties highly depend on temperature and frequency. Any small changes in these parameters may cause big differences in storage and loss modulus. The common way to specify complex modulus is to perform a dynamic mechanical analysis (DMA). In this technique, oscillating load is applied to viscoelastic material sample and response is measured. The correlation between oscillating stress and out of phase strain gives complex modulus of the material. Temperature and frequency sweep is also applied during analysis. Elastic characteristics of the hoses were not known before modal tests thus a DMA was required for them. In the scope of this thesis, hose samples are analyzed at a constant frequency with variable temperature and a constant temperature with variable frequency. These all results are given in Appendix A. Oscillating tension load was applied to hose specimen during DMA hence tensile modulus was acquired. Proper value for complex tensile modulus was selected according to temperature of the test VIM and foreseen middle value of the interested frequency range. The VIM temperature was about 23°C during test and 2 Hz frequency was taken into consideration as mid-value. However, only tensile modulus was not adequate to complete theoretical calculations. Complex shear modulus also had to be known because shear effects was included into the modified method. Thus, complex shear modulus was calculated by using basic relation between tensile modulus and shear modulus which is $G=E/2(1+v)$. Since the hose material was always in the rubbery region at stated temperature above, Poisson's value was assumed as 0.499. Required mechanical properties of the hose are listed in Table 4.1.

Table 4.1 Mechanical properties of the hose

E^*	33.4+4.43i MPa
ρ	1120 kg/m^3
ν	0.499

Stainless steel termination parts were attached to each end of the VIMs. Geometrical and inertial properties of them were obtained by means of CAD software. Mechanical properties of the stainless steel given in Table 4.2 were obtained from manufacturer.

Spacers were manufactured from polyacetal material. They were cylindrical in shape and outer surface of them always contacted with the inner face of the hose. Table 4.3 presents mechanical properties of the spacers. Likewise termination parts, properties of the spacers were provided by the row material manufacturer.

Table 4.2 Mechanical properties of the termination parts

E	193 GPa
ρ	8000 kg/m^3
ν	0.275

Table 4.3 Mechanical properties of the spacers

E	2.86 GPa
ρ	1420 kg/m^3
ν	0.35

Last component was the inner fluid which was filled until no air gap left inside the hose. Since the aim of using inner fluid was to provide neutral buoyancy, it had to have lower density than water. So, oil-based fluid whose density is given in following Table 4.4 was preferred. This value was taken from catalogue of supplier.

Table 4.4 Density of the inner fluid

ρ	784 kg/m^3

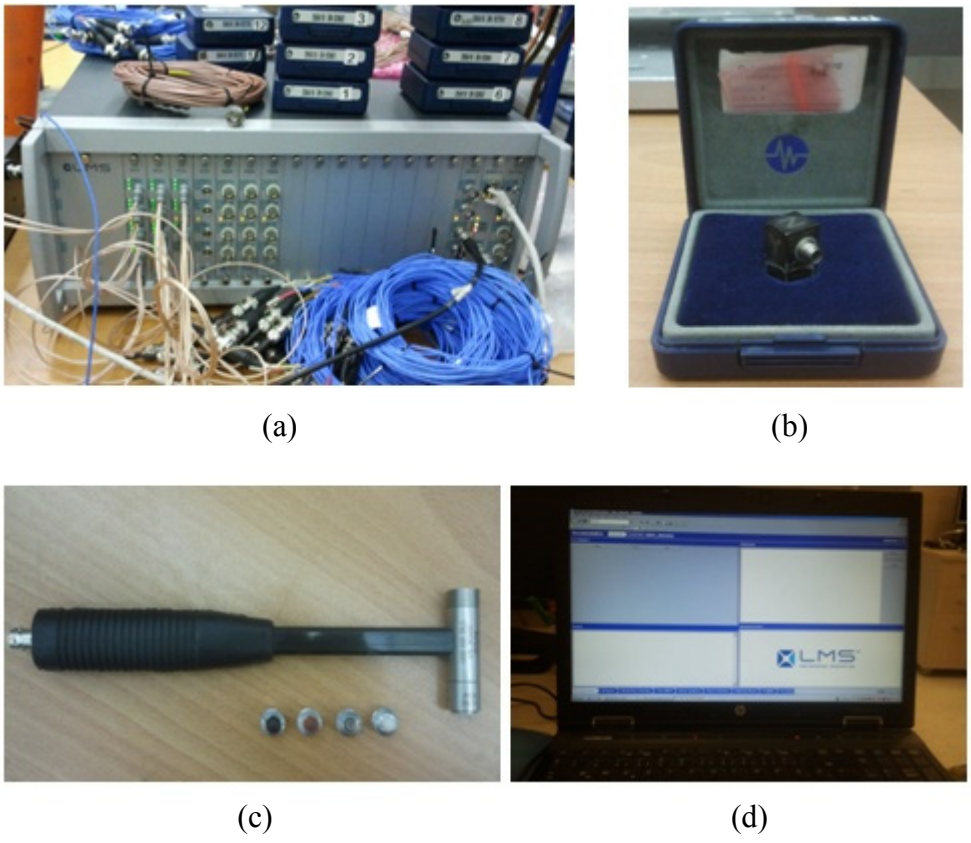

(a) (b)

(c) (d)

Figure 4.9 (a) Data acquisition system, (b) triaxial accelerometer, (c) impact hammer, (d) post-processing software

In the modal impact tests, PCB 356A16 model triaxial accelerometers were utilized to measure response. Sensitivities of these accelerometers are 10.2mV/(m/s^2) with a tolerance of ±10% and frequency range of them is between 0.5Hz and 5000Hz. Structures were excited by impact hammer with PCB 086C04 model load cell at its tip. Sensitivities of the load cell is 1.1mV/N with a tolerance of ±15%. Both input force and output acceleration information were sent to totally 60 channel LMS SCADAS data acquisition system. Cut-off frequency of the A/C coupling high pass filter is 0.5Hz. Collected data were sampled at the frequency of 512Hz and FRFs were generated by this acquisition system. Lastly, all FRFs were evaluated in the post processor software which is LMS Test Lab and desired modal parameters were calculated. All these test equipments are demonstrated in Figure 4.9, respectively.

Ten accelerometers were attached to the VIM, especially onto the termination parts and spacers. Numbers of the accelerometers began from one at the bottom end and increased at upward direction. It was endeavored that all accelerometers were align. Afterwards, impact was applied to a single point which located at the opposite side of the first accelerometer on the bottom termination part. Impact action was repeated in fifteen times to increase the accuracy of the collected data. In case of double hit or overload, the hit was rejected automatically and extra hit was performed instead. Although triaxial accelerometers were used, only accelerations in one direction were measured during test. After that, data acquisition system applied data windows to the acquired impulse and response signals after sampling. Force window was use to eliminate noise on impulse signal whereas exponential window was for response signal to minimize the leakage at frequency domain. FRFs were generated with curve-fitting methods transferred to LMS Test Lab software. At the end, resonance frequencies with damping ratios were defined and mode shapes were visualized in this software. Simple drawings of the VIM, VIM setup and whole test setup are represented in Figure 4.10 and Figure 4.11 below, respectively.

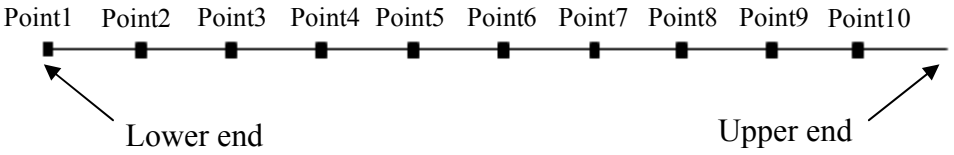

(a)

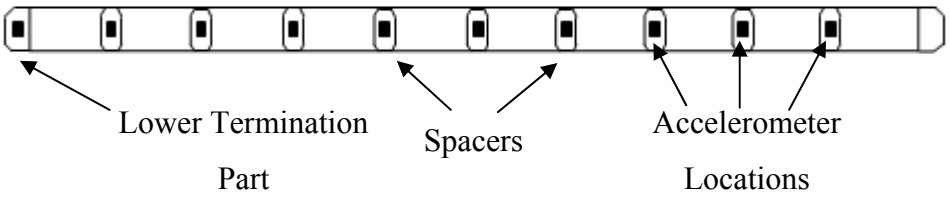

(b)

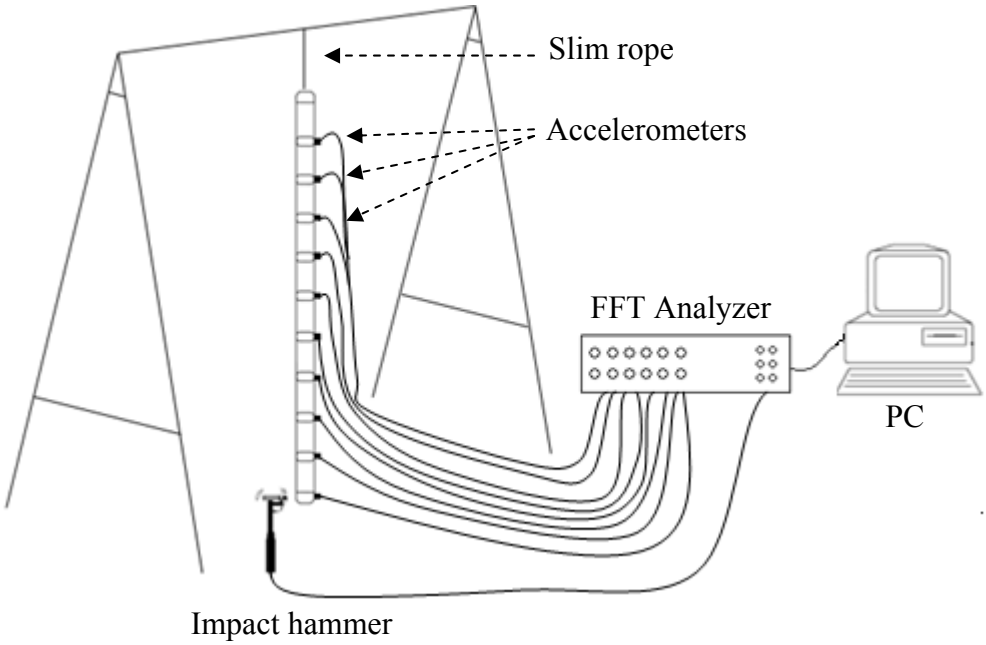

(c)

Figure 4.10 (a) LMS Test Lab VIM model, (b) simple drawing of the VIM and (c) modal test setup of the VIM

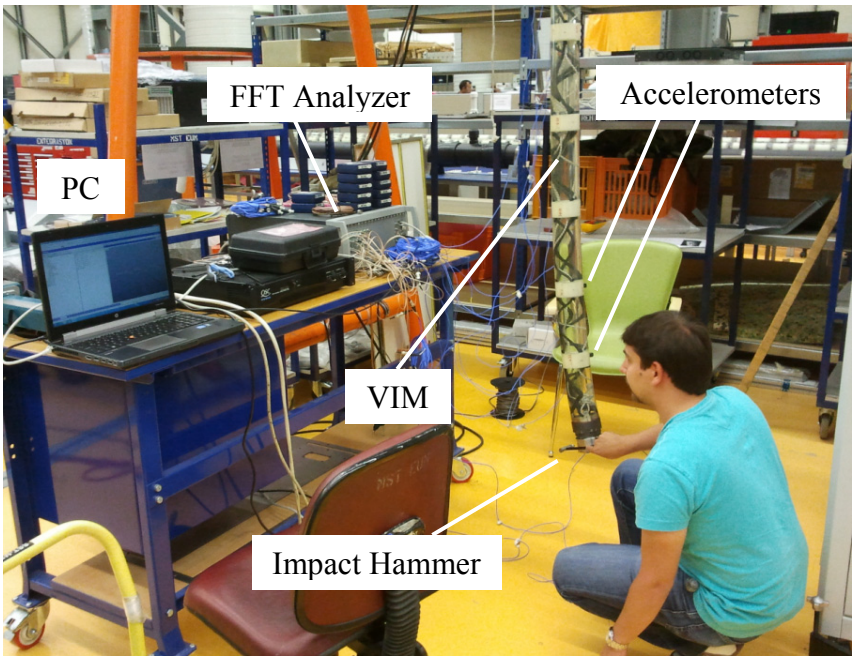

Figure 4.11 Modal impact test of the hanged VIM

4.3 Results of the VIM Test

Developed theoretical model works to find out only bending natural frequencies of the structures. Accordingly, test results are evaluated in this perspective. Whether the resonance frequency is bending or not is designated by checking the relevant mode shape. The first three resonance frequencies out of test are given in the following Table 4.5.

Table 4.5 Resonance frequencies of the VIM sample

	ω_1	ω_2	ω_3
Resonance Frequency (Hz)	2.736	4.216	7.802

Mode shapes are displayed at Figure 4.12 where the first three bending mode of the VIM are in sequence. It is obvious from mode shapes that the hung VIM carries the characteristic of a beam with a free-free boundary condition. Locations of the accelerometers are designated as point.

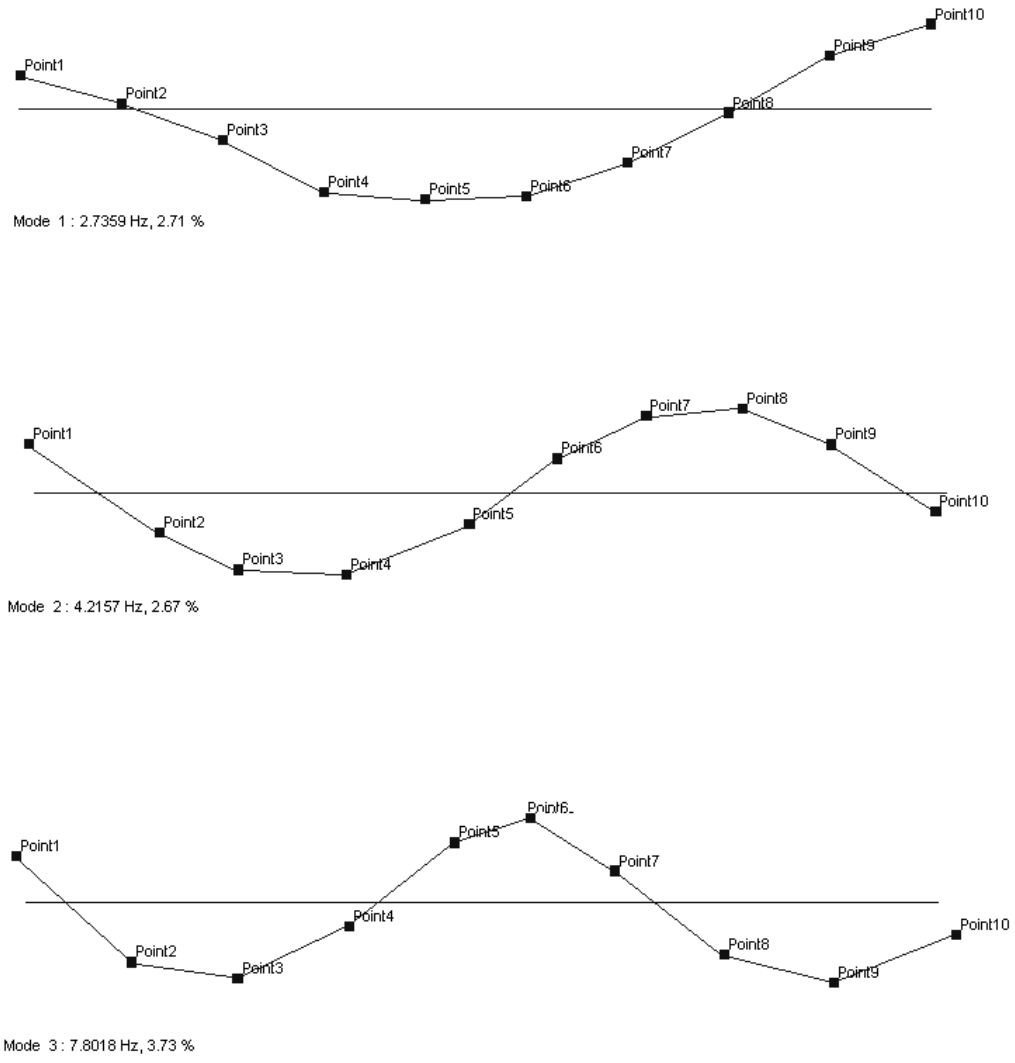

Figure 4.12 The first three bending mode of VIM sample

On the other hand, examination of the FRF and coherence graphics is required to evaluate results in a correct manner.

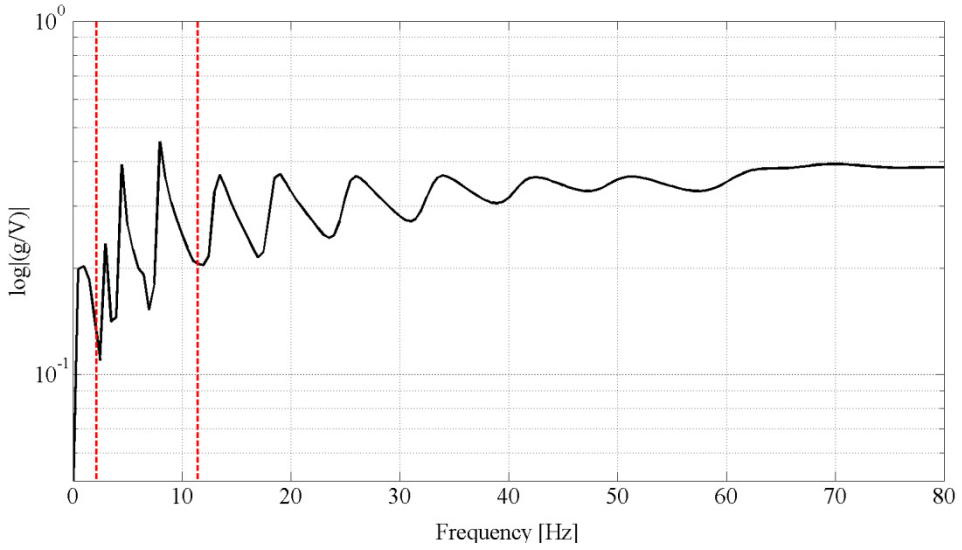

(a)

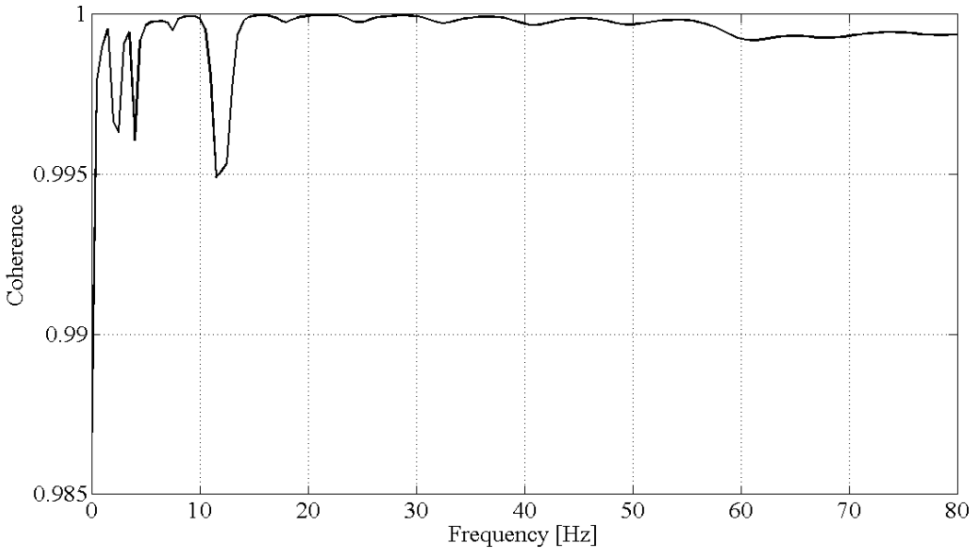

(b)

Figure 4.13 (a) FRF and (b) Coherence graphics according to the first accelerometer

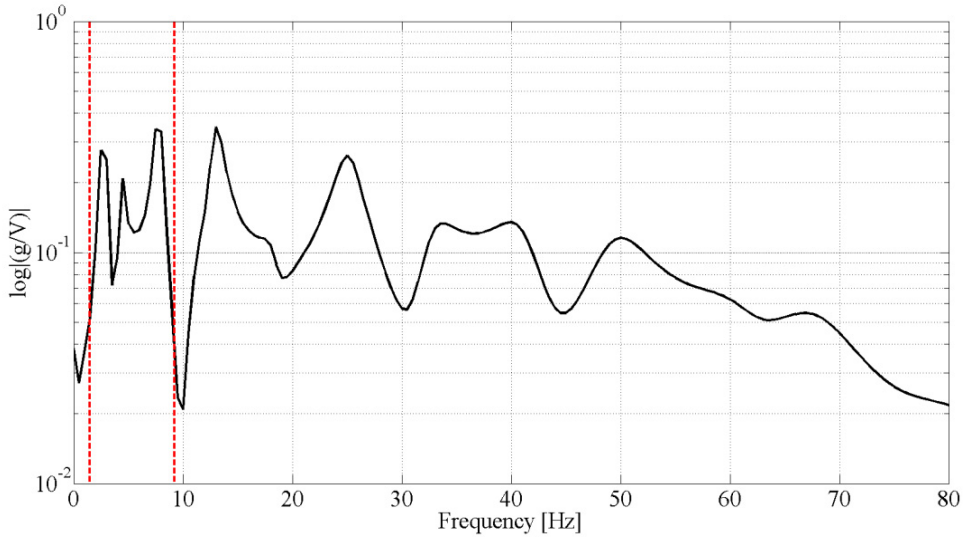

(a)

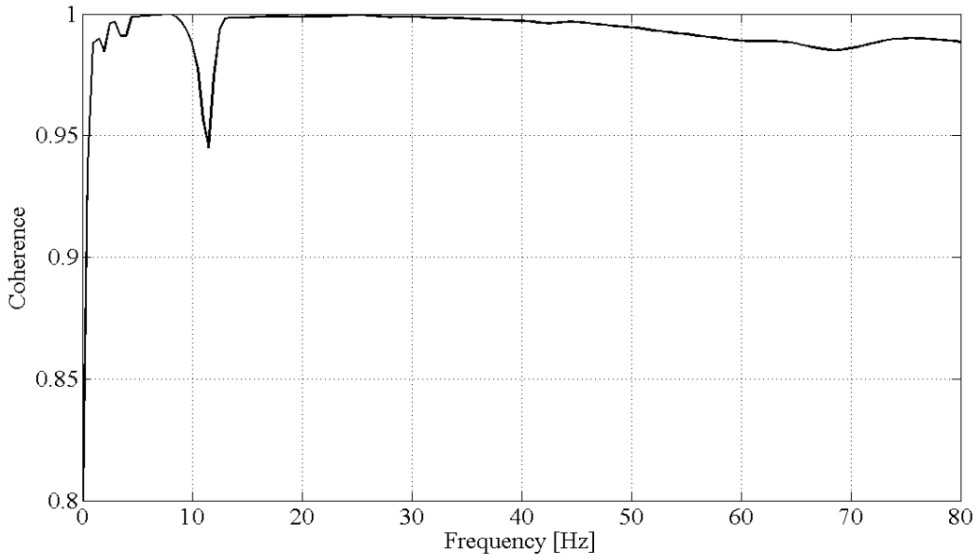

(b)

Figure 4.14 (a) FRF and (b) Coherence graphics according to the fifth accelerometer

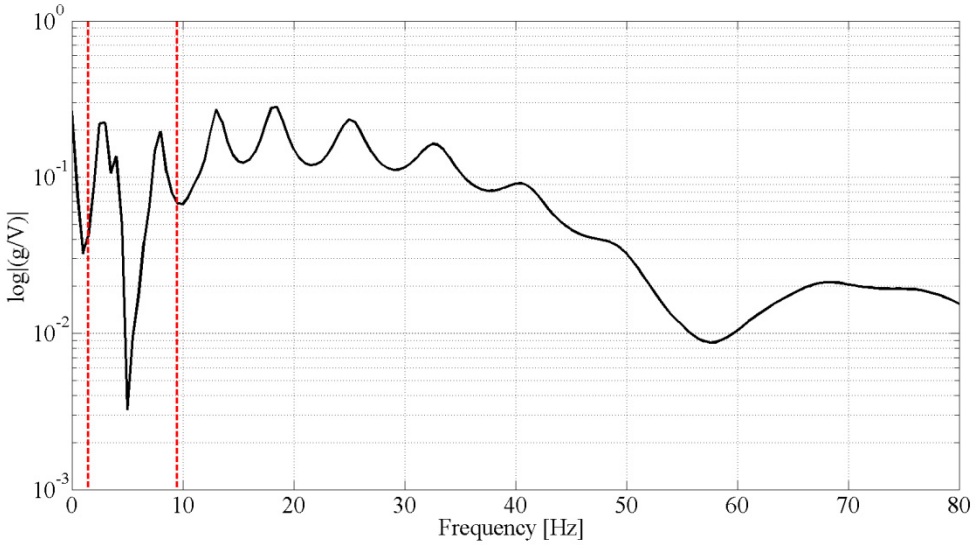

(a)

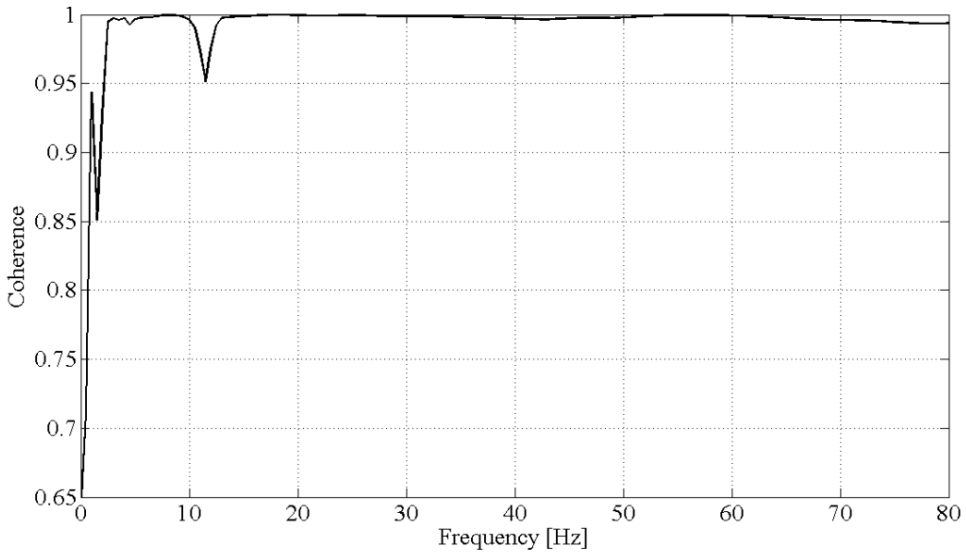

(b)

Figure 4.15 (a) FRF and (b) Coherence graphics according to the tenth accelerometer

Due to the single input and ten outputs, there exist ten FRFs. However, it is adequate to represent three of them which belong to the first, fifth and tenth accelerometers. Figure 4.13a, Figure 4.14a and Figure 4.15a show the graphics of these three FRFs. The FRF graphics are quite clear and peaks at resonance are apparent. Interested resonance frequencies are stated between red dashed lines. Certain resonance frequencies are picked up after some stabilization algorithm on FRFs by LMS Test Lab software. Apart from bending modes, suspension modes occurred at low frequencies for hung systems. These modes most probably appeared at around 0.5 Hz or lower. Hence, they could not be identified from FRFs because of the high-pass filter cut-off frequency and the minimum measurement capacity of the accelerometers.

Only FRFs are not sufficient to draw conclusion. Coherences must be checked to see quality of the measurements. Simply, coherence gives an idea about quality of input-output relation. For instance, existence of noise or another unwanted excitation sources can be realized. Coherence values vary between 0 and 1. For modal test, coherence under the value of 0.7 is not acceptable. In this VIM test, coherence values which are indicated in Figure 4.13b, Figure 4.14b and Figure 4.15b are considerably satisfactory at interested frequency band. In common with FRFs, coherences between the input and three outputs will be shown above but general trend is the same for all outputs.

Experimental studies and results were told in this chapter. Comparison between theoretical results and test results will be handled in the next chapter. Moreover, differences will be discussed and interpreted on the bases of ANSYS model.

CHAPTER 5

THEORETICAL RESULTS AND MODEL VALIDATION

In this chapter, firstly, validation of the mathematical model in Chapter 3 will be examined. Reliability of the model will be shown by applying various boundary conditions and determining optimum number of segment. Results will be compared with FEM solution by means of ANSYS software. After that, natural frequencies of the hung VIM will be calculated by using the modified model.

5.1 Verification of Modified Myklestad`s Method

For the verification of the modified Myklestad`s Method mentioned in Chapter 3, a steel tube having length of 2.8m, outer diameter of 0.09 m and inner diameter of 0.08 m (Figure 5.1) will be handled. Seven different boundary conditions will be applied this tube and the first four natural frequencies in bending will be obtained. Seven boundary conditions are indicated at Figure 5.1 as follows.

Figure 5.1 A steel tube sample

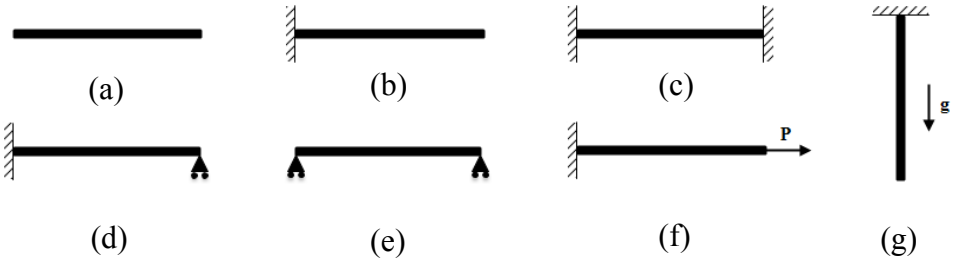

Figure 5.2. (a) Free – Free Condition, (b) Clamped – Free Condition, (c) Clamped – Clamped Condition, (d) Clamped – Simply Supported Condition, (e) Simply Supported – Simply Supported Condition, (f) Clamped – Free Under Constant Tension Condition, (g) Clamped – Free Under Gravity

The reason why these geometric dimensions for sample are selected is to liken the sample to the tested VIM model. Mechanical properties of steel are provided in Table 5.1.

Table 5.1 Mechanical properties of steel

Density	7850 kg/m^3
Modulus of Elasticity	200 GPa
Poisson`s Ratio	0.3

Approximate shear coefficient for hollow cylinders can be calculated by using below equation [45]

$$\kappa = \frac{2(1+\nu)}{(4+3\nu)} \tag{5.1}$$

Additionally, during verification stage, various segment numbers will be tried and minimum segment number for adequate accuracy will be defined by controlling the difference.

5.1.1 Free – Free Boundary Conditions

At free – free boundary condition state, both shear force and moment are zero at the each end. So, the relation between the contrary ends can be written in matrix form as;

$$\begin{bmatrix} y \\ \psi \\ 0 \\ 0 \end{bmatrix}_n^R = \begin{bmatrix} u_{11}(\omega) & u_{12}(\omega) & u_{13}(\omega) & u_{14}(\omega) \\ u_{21}(\omega) & u_{22}(\omega) & u_{23}(\omega) & u_{24}(\omega) \\ u_{31}(\omega) & u_{32}(\omega) & u_{33}(\omega) & u_{34}(\omega) \\ u_{41}(\omega) & u_{42}(\omega) & u_{43}(\omega) & u_{44}(\omega) \end{bmatrix}_n \begin{bmatrix} y \\ \psi \\ 0 \\ 0 \end{bmatrix}_0^R \tag{5.2}$$

The ω values which satisfy all boundary conditions above are calculated from determinant of 2x2 matrix.

$$\begin{bmatrix} 0 \\ 0 \end{bmatrix}_n^R = \begin{bmatrix} u_{31}(\omega) & u_{32}(\omega) \\ u_{41}(\omega) & u_{42}(\omega) \end{bmatrix}_n \begin{bmatrix} y \\ \psi \end{bmatrix}_0^R \tag{5.3}$$

$$\det \begin{bmatrix} u_{31}(\omega) & u_{32}(\omega) \\ u_{41}(\omega) & u_{42}(\omega) \end{bmatrix} = 0 \tag{5.4}$$

It must be noted that, number of the available natural frequencies is directly proportional to number of segments.

The first four natural frequencies in bending were calculated for free – free boundary conditions by changing in number of segments and results were compared with FEM results. Computations were performed by aid of MATLAB software. Comparisons of natural frequencies and differences are presented in Table 5.2, Table 5.3, Table 5.4 and Table 5.5.

Table 5.2 The first four natural frequencies for free - free boundary conditions.
Number of Segments=10

Natural Frequency	Modified Myklestad`s Method (Hz)	FEM (Hz)	Difference (%)
ω_1	69.639	68.525	1.626
ω_2	191.318	186.44	2.616
ω_3	370.452	358.68	3.282
ω_4	598.272	578.82	3.361

Table 5.3 The first four natural frequencies for free - free boundary conditions.
Number of Segments=100

Natural Frequency	Modified Myklestad`s Method (Hz)	FEM (Hz)	Difference (%)
ω_1	68.592	68.525	0.098
ω_2	186.731	186.44	0.156
ω_3	359.522	358.68	0.235
ω_4	580.717	578.82	0.328

Table 5.4 The first four natural frequencies for free - free boundary conditions. Number of Segments=500

Natural Frequency	Modified Myklestad`s Method (Hz)	FEM (Hz)	Difference (%)
ω_1	68.582	68.525	0.083
ω_2	186.688	186.44	0.133
ω_3	359.416	358.68	0.205
ω_4	580.529	578.82	0.295

Table 5.5 The first four natural frequencies for free - free boundary conditions. Number of Segments=1000

Natural Frequency	Modified Myklestad`s Method (Hz)	FEM (Hz)	Difference (%)
ω_1	68.582	68.525	0.083
ω_2	186.686	186.44	0.132
ω_3	359.413	358.68	0.204
ω_4	580.523	578.82	0.294

In the light of above calculations, there are quite small differences between natural frequencies when the numbers of segments are taken as 500 and 1000. Thus, it can be stated that natural frequency values converge at about 500 segments. This number of segment is going to be taken into consideration for all other boundary conditions and real VIM structures.

5.1.2 Clamped – Free Boundary Conditions

Boundary conditions at the clamped end can be described as both displacement and slope are zero. As mentioned above, moment and shear force are zero for free end boundary conditions. The following matrix relation connects two opposite ends

$$\begin{bmatrix} y \\ \psi \\ 0 \\ 0 \end{bmatrix}_n^R = \begin{bmatrix} u_{11}(\omega) & u_{12}(\omega) & u_{13}(\omega) & u_{14}(\omega) \\ u_{21}(\omega) & u_{22}(\omega) & u_{23}(\omega) & u_{24}(\omega) \\ u_{31}(\omega) & u_{32}(\omega) & u_{33}(\omega) & u_{34}(\omega) \\ u_{41}(\omega) & u_{42}(\omega) & u_{43}(\omega) & u_{44}(\omega) \end{bmatrix}_n \begin{bmatrix} 0 \\ 0 \\ M \\ V \end{bmatrix}_0^R \tag{5.5}$$

Natural frequencies which satisfy above boundary conditions can be found out by extracting 2x2 matrix and taking determinant of it.

$$\begin{bmatrix} 0 \\ 0 \end{bmatrix}_n^R = \begin{bmatrix} u_{33}(\omega) & u_{34}(\omega) \\ u_{43}(\omega) & u_{44}(\omega) \end{bmatrix}_n \begin{bmatrix} M \\ V \end{bmatrix}_0^R \tag{5.6}$$

$$\det \begin{bmatrix} u_{33}(\omega) & u_{34}(\omega) \\ u_{43}(\omega) & u_{44}(\omega) \end{bmatrix} = 0 \tag{5.7}$$

Results about to steel tube which is fixed at left and free at right end are given in the following Table 5.6.

Table 5.6 The first four natural frequencies for clamped - free boundary conditions. Number of Segments=500

Natural Frequency	Modified Myklestad`s Method (Hz)	FEM (Hz)	Difference (%)
ω_1	10.807	10.821	0.129
ω_2	67.098	67.154	0.083
ω_3	185.149	185.18	0.017
ω_4	355.459	355.2	0.073

5.1.3. Clamped – Clamped Boundary Conditions

It is known from previous sections that displacement and slope are both zero for clamped ends. Overall transfer matrix along tube and state vectors at each end are given by the equation below.

$$\begin{bmatrix} 0 \\ 0 \\ M \\ V \end{bmatrix}_n^R = \begin{bmatrix} u_{11}(\omega) & u_{12}(\omega) & u_{13}(\omega) & u_{14}(\omega) \\ u_{21}(\omega) & u_{22}(\omega) & u_{23}(\omega) & u_{24}(\omega) \\ u_{31}(\omega) & u_{32}(\omega) & u_{33}(\omega) & u_{34}(\omega) \\ u_{41}(\omega) & u_{42}(\omega) & u_{43}(\omega) & u_{44}(\omega) \end{bmatrix}_n \begin{bmatrix} 0 \\ 0 \\ M \\ V \end{bmatrix}_0^R \tag{5.8}$$

The part of the overall transfer matrix in order to calculate natural frequencies is;

$$\begin{bmatrix} 0 \\ 0 \end{bmatrix}_n^R = \begin{bmatrix} u_{13}(\omega) & u_{14}(\omega) \\ u_{23}(\omega) & u_{24}(\omega) \end{bmatrix}_n \begin{bmatrix} M \\ V \end{bmatrix}_0^R \tag{5.9}$$

Determinant of above 2x2 matrix gives desired results.

$$\det\begin{bmatrix} u_{13}(\omega) & u_{14}(\omega) \\ u_{23}(\omega) & u_{24}(\omega) \end{bmatrix} = 0 \tag{5.10}$$

Natural frequencies for clamped - clamped boundary conditions found by using Modified Myklestad`s Method and FEM are compared at Table 5.7.

Table 5.7 The first four natural frequencies for clamped - clamped boundary conditions. Number of Segments=500

Natural Frequency	**Modified Myklestad`s Method (Hz)**	**FEM (Hz)**	**Difference (%)**
ω_1	68.021	67.926	0.14
ω_2	184.182	183.77	0.224
ω_3	352.947	351.81	0.323
ω_4	567.771	565.32	0.434

5.1.4 Clamped – Simply Supported Boundary Conditions

This time, unlike clamped and free boundary conditions, simply supported boundary condition becomes involved in solution period. Displacement and moment are always zero for simply supported boundary condition. So, state vector owing simply supported end and over all transfer matrix can be expressed as;

$$\begin{bmatrix} 0 \\ \psi \\ 0 \\ V \end{bmatrix}_n^R = \begin{bmatrix} u_{11}(\omega) & u_{12}(\omega) & u_{13}(\omega) & u_{14}(\omega) \\ u_{21}(\omega) & u_{22}(\omega) & u_{23}(\omega) & u_{24}(\omega) \\ u_{31}(\omega) & u_{32}(\omega) & u_{33}(\omega) & u_{34}(\omega) \\ u_{41}(\omega) & u_{42}(\omega) & u_{43}(\omega) & u_{44}(\omega) \end{bmatrix}_n \begin{bmatrix} 0 \\ 0 \\ M \\ V \end{bmatrix}_0^R \tag{5.11}$$

The first and third rows element intersecting with the third and fourth columns constitute solution matrix. Again taking determinant, natural frequencies will be obtained.

$$\begin{bmatrix} 0 \\ 0 \end{bmatrix}_n^R = \begin{bmatrix} u_{13}(\omega) & u_{14}(\omega) \\ u_{33}(\omega) & u_{34}(\omega) \end{bmatrix}_n \begin{bmatrix} M \\ V \end{bmatrix}_0^R \tag{5.12}$$

$$\det \begin{bmatrix} u_{13}(\omega) & u_{14}(\omega) \\ u_{33}(\omega) & u_{34}(\omega) \end{bmatrix} = 0 \tag{5.13}$$

From the Table 5.8, it can be easily seen that differences between two methods are quite small.

Table 5.8 The first four natural frequencies for clamped – simply supported boundary conditions. Number of Segments=500

Natural Frequency	**Modified Myklestad`s Method (Hz)**	**FEM (Hz)**	**Difference (%)**
ω_1	47.167	47.117	0.106
ω_2	150.76	150.51	0.166
ω_3	308.481	307.7	0.254
ω_4	514.815	513	0.354

5.1.5 Simply Supported – Simply Supported Boundary Conditions

By applying the simply supported boundary condition to the left end, equation (5.11) can be rearranged for simply supported – simply supported end conditions. Rearranged matrix equation one end to other form is given below.

$$\begin{bmatrix} 0 \\ \psi \\ 0 \\ V \end{bmatrix}_n^R = \begin{bmatrix} u_{11}(\omega) & u_{12}(\omega) & u_{13}(\omega) & u_{14}(\omega) \\ u_{21}(\omega) & u_{22}(\omega) & u_{23}(\omega) & u_{24}(\omega) \\ u_{31}(\omega) & u_{32}(\omega) & u_{33}(\omega) & u_{34}(\omega) \\ u_{41}(\omega) & u_{42}(\omega) & u_{43}(\omega) & u_{44}(\omega) \end{bmatrix}_n \begin{bmatrix} 0 \\ \psi \\ 0 \\ V \end{bmatrix}_0^R \tag{5.14}$$

Sub-matrix require to figure out natural frequencies can be extracted from the first and the third rows.

$$\begin{bmatrix} 0 \\ 0 \end{bmatrix}_n^R = \begin{bmatrix} u_{12}(\omega) & u_{14}(\omega) \\ u_{32}(\omega) & u_{34}(\omega) \end{bmatrix}_n \begin{bmatrix} \psi \\ V \end{bmatrix}_0^R \tag{5.15}$$

$$\det \begin{bmatrix} u_{12}(\omega) & u_{14}(\omega) \\ u_{32}(\omega) & u_{34}(\omega) \end{bmatrix} = 0 \tag{5.16}$$

Calculated natural frequencies and FEM results are available in Table 5.9.

Table 5.9 The first four natural frequencies for simply supported – simply supported boundary conditions. Number of Segments=500

Natural Frequency	Modified Myklestad`s Method (Hz)	FEM (Hz)	Difference (%)
ω_1	30.343	30.318	0.082
ω_2	120.177	120.03	0.122
ω_3	266.121	265.61	0.192
ω_4	463.133	461.83	0.282

5.1.6 Clamped – Free Boundary Conditions Under Constant Tension

Modified Myklestad`s Method in Chapter 3 takes account of tension force in calculations. In order to verify above boundary conditions, tension force has been taken as zero value from section 5.1.1 to 5.1.5. However, to demonstrate adaptability of the method for all conditions, theoretical and FEM natural frequencies of steel tube under tension will be examined in this section. Three tension loads which are 10000N, 30000N and 50000N will be applied and results will be given in Table 5.10, Table 5.11 and Table 5.12, respectively.

The steel tube is modeled as lying horizontally. Left hand side is clamped and right hand side free but pulled with a constant force (Figure 5.2f). Since boundary conditions are the same with section 5.1.2 condition, the same state vectors and overall transfer matrix can be utilized fully for this condition. Related results are as follows;

Table 5.10 The first four natural frequencies for clamped - free boundary conditions under 10000N tension. Number of Segments=500

Natural Frequency	Modified Myklestad`s Method (Hz)	FEM (Hz)	Difference (%)
ω_1	11.441	11.457	0.14
ω_2	67.821	67.885	0.094
ω_3	185.758	185.81	0.028
ω_4	356.023	355.8	0.063

Table 5.11 The first four natural frequencies for clamped - free boundary conditions under 30000N tension. Number of Segments=500

Natural Frequency	Modified Myklestad`s Method (Hz)	FEM (Hz)	Difference (%)
ω_1	12.587	12.606	0.151
ω_2	69.241	69.321	0.115
ω_3	186.969	187.06	0.049
ω_4	357.147	356.99	0.044

Table 5.12 The first four natural frequencies for clamped - free boundary conditions under 50000N tension. Number of Segments=500

Natural Frequency	Modified Myklestad`s Method (Hz)	FEM (Hz)	Difference (%)
ω_1	13.606	13.629	0.169
ω_2	70.628	70.723	0.134
ω_3	188.172	188.3	0.068
ω_4	358.269	358.18	0.025

As it is seen, tension increases the stiffness of the structure. Naturally, any improvement on stiffness enhances the natural frequency. Such in previous boundary condition states, differences between results are quite satisfactory for tension condition as well.

5.1.7 Clamped – Free Boundary Conditions Under the Gravitational Force

In section 5.1.6, constant force on steel tube was studied. In other words, the tension was always a constant value at any point on tube. However, this tension force cannot be constant for all times. Hanged and sufficiently long structures can be indicated as examples of varying tension force through structures owing to gravitation.

Here, steel tube is going to be hanged at its upper end and below end will be free. This time, gravitation will not be neglected as before, so that tension on tube begins from zero value at below end and increases gradually towards upper end. Magnitude of the tension force at any point on tube will be equal to weight of the portion between selected point and below end. Thus, while maximum tension occurs at upper and minimum tension appears on below end having zero value.

As shown in Figure 5.2g, clamped boundary condition for upper end and free boundary condition for below end are valid. Hence, again state vectors and overall transfer matrix in section 5.1.2 are appropriate for hanged steel tube.

During calculation, tension force for each segment is varying. The tension difference between two consecutive segments is equal to weight of the segment. Results from Modified Myklestad`s Method and FEM are compared at following Table 5.13.

Table 5.13 The first four natural frequencies for clamped - free boundary conditions under gravitational force. Number of Segments=500

Natural Frequency	**Modified Myklestad`s Method (Hz)**	**FEM (Hz)**	**Difference (%)**
ω_1	10.813	10.827	0.129
ω_2	67.103	67.16	0.085
ω_3	185.154	185.19	0.019
ω_4	355.465	355.21	0.072

Differences are again considerably small when two methodologies are compared. As a consequences of above seven different boundary condition states, the Modified Myklestad`s Method has been verified for natural frequencies of transverse vibration. After above verification procedures from section 5.1.1, the method can be confidently utilized to determine bending natural frequencies of VIM structures.

5.2 Natural Frequencies of the Hung VIM

As stated in Chapter 4, the VIM was hanged to the overhead winch frame in the laboratory with a slim rope from its upper end whereas the below end was free. The VIM lies vertically and tension forces along structures vary due to gravitation. So, conditions of the VIM resemble to verification problem in section 5.1.7 in terms of tension force distribution but boundary conditions are distinct. The upper ends were not exactly free but these ends can be assumed as free because of the slim rope. On the basis of this assumption, state vectors and overall transfer matrix in section 5.1.1 are appropriate for the VIMs by inserting the variable tension forces in calculations.

Stainless steel termination parts, thermoplastic hose, POM spacers and filling oil are components of the VIM. Related geometrical and mechanical properties of all components were given in Chapter 4. In the VIM, spacers were placed with 22cm intervals. Distances from termination part to spacer and from spacer to spacer are almost the same.

In calculations, only inertial properties of the internal fluid will be taken into consideration. Also, although the internal fluid fills every void through the hose, fluid inside the center holes of spacers and termination parts will be neglected.

Steel termination parts and POM spacers can be assumed as pure elastic materials. Hose, however, is a viscoelastic material so that it shows both elastic and viscous characteristics naturally. That`s why, dynamic modulus describes the elastic properties of the hose more accurate than modulus of elasticity. In fact, using dynamic modulus means that structural damping will be taken into account. Roots from the equation of motion of damped structures will also become complex values as follows.

$$\lambda^2 = \omega_n^2 (1 + i\eta) \tag{5.17}$$

where λ^2 is eigenvalue, ω_n is natural frequency and η is loss factor. At resonance frequency, equation (5.18) expresses the relation between loss factor and damping ratio.

$$\zeta = \frac{\eta}{2} \tag{5.18}$$

The VIM is 2.79 m in length. VIM will be divided into 558 segments thus the length of each segment will be 0.005m. It can be obviously seen from verification problems throughout section 5.1 that 500 or higher number of segments gives considerably good results. Segments on the VIM structure are demonstrated in Figure 5.3 below.

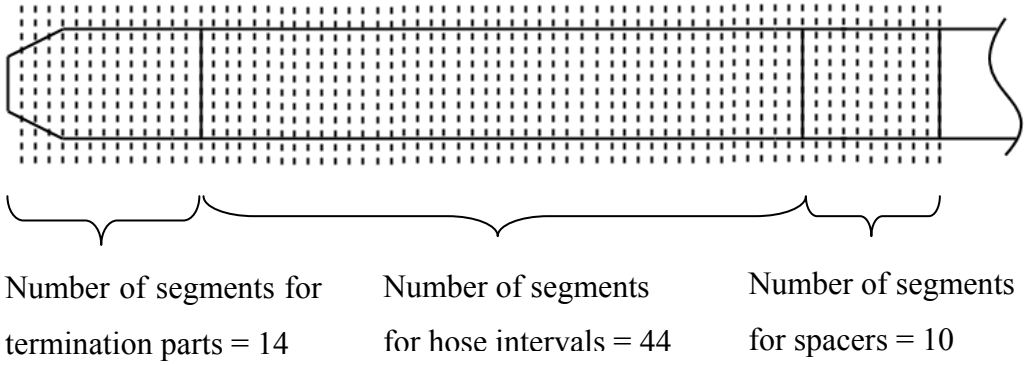

Figure 5.3. Number of segments for each element in the first VIM

Calculation procedure will be the same as previous verification problems. Firstly, state vectors and overall transfer matrix will be generated. According to free – free boundary condition state, 2x2 matrix will be extracted to be able to find out natural frequencies of the structure. However, roots from determinant of this 2by 2 matrix would have complex value due to dynamic modulus of the hose. Square of the roots which was stated in equation (5.17) would give all information about natural

frequencies and damping ratios. As a result of calculations, the first three bending natural frequencies belonging to the first VIM structure are represented in Table 5.14.

Table 5.14 The first three bending natural frequencies of the first VIM

Theoretical Results				
	λ_n	$\lambda_n^2=\omega_{n_2}^2+i\eta_n\omega_n$	ω_n **(Hz)**	η_n
1	1.744 + 0.0454i	3.0409 + 0.158i	1.744	0.052
2	3.774 + 0.1703i	14.216 + 1.286i	3.77	0.09
3	6.903 + 0.3772i	47.508 + 5.208i	6.892	0.11

Table 5.15 Comparison of the experimental and theoretical results

	Theoretical Results (Hz)	**Experimental Results (Hz)**	**Error %**
ω_1	1.744	2.736	57
ω_2	3.77	4.216	12
ω_3	6.892	7.802	13

When the theoretical results are compared with the experimental results (Table 5.15), one can consider that modified mathematical model is not acceptable solution. The errors are substantially high. However, it was observed that some conditions or parameters which were excluded in the analysis affect the results significantly. Next section will explain these conditions and parameters in order and show the validation of the mathematical model for the VIM.

5.3 Assessment of the Theory and the Test

There must be reasonable explanations about differences between theoretical and experimental results, so there are. When the test conditions and test structure were examined in detail, sources of the differences were revealed.

First of all, free-free boundary conditions were taken into consideration while calculating the bending natural frequencies of the VIM theoretically. However, exact provision of these boundary conditions during test is not possible. The structure must be attached to anywhere with some supporting elements. Common method to simulate free-free boundary conditions during tests is to hang the test structure with considerably long and flexible ropes. One should be careful while defining the rope because properties of the rope may affect the dynamic behavior of the system.

As stated in the Chapter 4, the VIM was hung to the overhead winch frame with a rope. Due to the dimensions of the winch and the VIM, rope with 650mm length was used at maximum. Diameter and elastic modulus of the rope is 4mm and 120 GPa, respectively. In order to understand the effects of the used rope, two different analyses were run by means of a finite element software ANSYS. Firstly, the VIM was modeled as suspended with a very long spring to ideally simulate free-free conditions and apply the gravity (Figure 5.4a). After that, another model was built up with a spring which is 650mm in length in order to simulate the test conditions (Figure 5.4b). Moreover, longitudinal stiffness of this spring was determined by using properties of the rope. From the formula of EA/L, average longitudinal stiffness was calculated as 2320N/mm. Results of these two analyses in terms of the first three bending natural frequencies are given in Table 5.16.

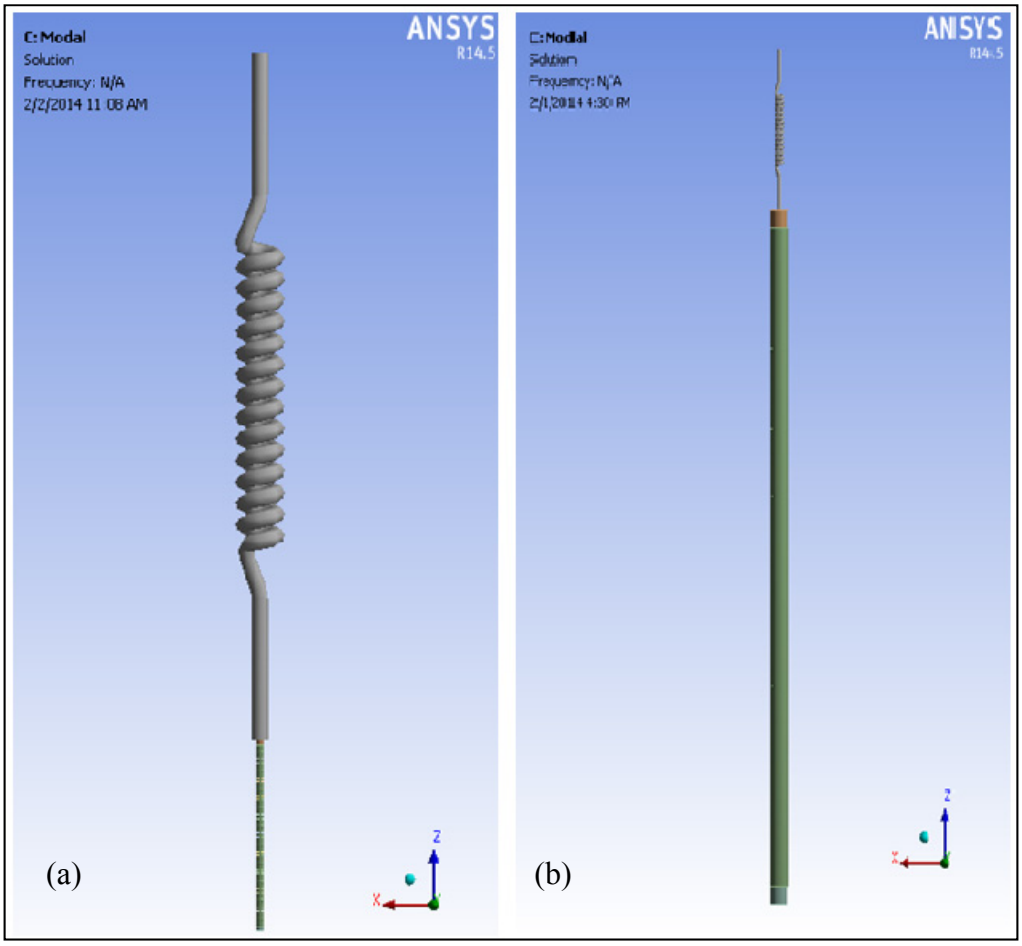

Figure 5.4 (a) VIM model with a long spring, (b) VIM model with a spring with 650mm long and 2320N/mm longitudinal stiffness

Table 5.16 The first three bending natural frequencies of VIM models

	VIM with long spring	**VIM with 650mm long spring**	**Difference %**
ω_1	1.669 Hz	1.93 Hz	15.64
ω_2	3.594 Hz	3.682 Hz	2.45
ω_3	6.633 Hz	6.665 Hz	0.48

Since the VIM is symmetric, natural frequencies occur in pairs and mode shapes are identical but occur at perpendicular planes. Thus, one of the double frequencies for each mode shape was stated in Table 5.16. It can be easily noticed from above table that boundary with a short rope is quite influential on the first bending natural frequency in which 15.64% difference exists. However, the second and the third bending natural frequencies are not affected from this boundary condition too much. While the difference in the second frequency is about 2.5%, this ratio becomes 0.48% for the third frequency.

Another interpretation about the effect of the test rope can be made over the mode shape. As a result of the ANSYS solution for 650mm long spring, upper tip of the VIM which is attached to the rope deflects more than the below tip. This deflection can be seen in the right hand side of the Figure 5.5. The same effect was observed in test, as well. Point 10 of the first mode shape in Figure 4.12 deflected more than Point 1. Hence, these analyses explain the rope effect clearly.

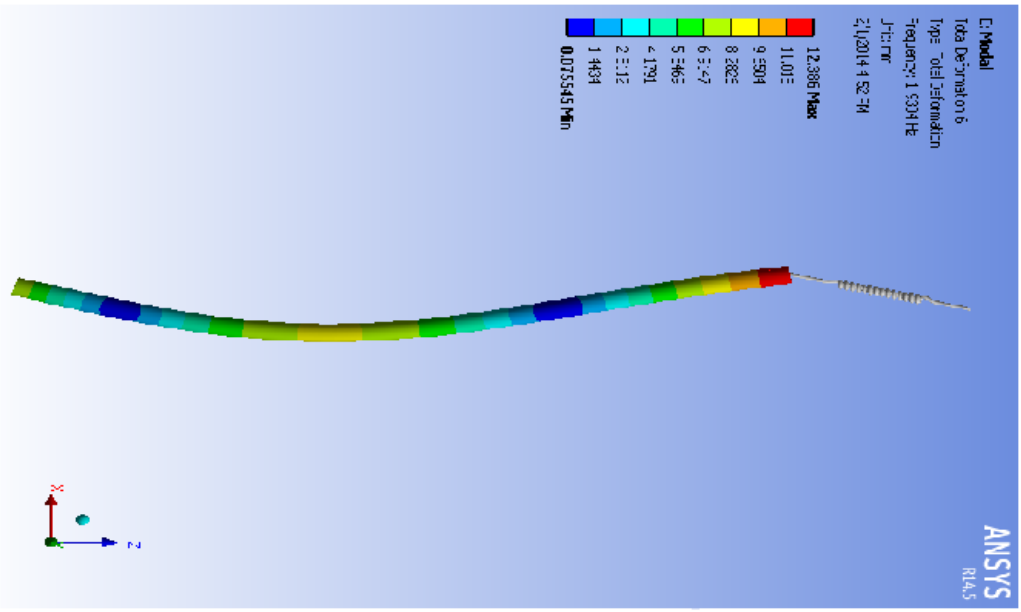

Figure 5.5 The first bending mode of VIM with 650mm long spring

Throughout the theoretical calculations, the VIM was assumed as being straight. However, the test specimen which is shown in Figure 5.6 was in curved form because of stocking on tambour. Being curved was not covered by the mathematical model which was presented in the Chapter 3. So, two different analyses were conducted with ANSYS to determine the effects of being curved on natural frequencies. Initially, a straight VIM was modeled in ANSYS. After calculating the natural frequencies of this model, a curved beam was generated and analyzed (Figure 5.7). Curvature dimension of the ANSYS model was almost similar to the test VIM. During analyses, gravity was not applied because some errors were encountered when the curved model was suspended with spring. Thus, only inertial properties were taken into consideration. At the end of the analyses some interesting results occurred. It was expected that natural frequencies of the curved model would not be double because the structure was not symmetric anymore. Nevertheless, it was observed that only the first bending modes on perpendicular planes were distinct and other modes were again double. Analysis results are given in Table 5.17.

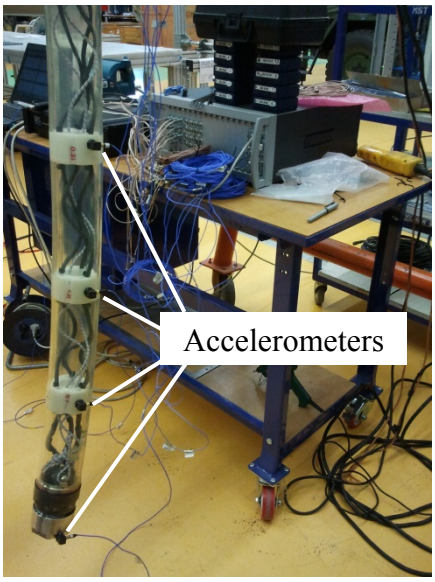

Figure 5.6 Curvature of the VIM and accelerometers locations

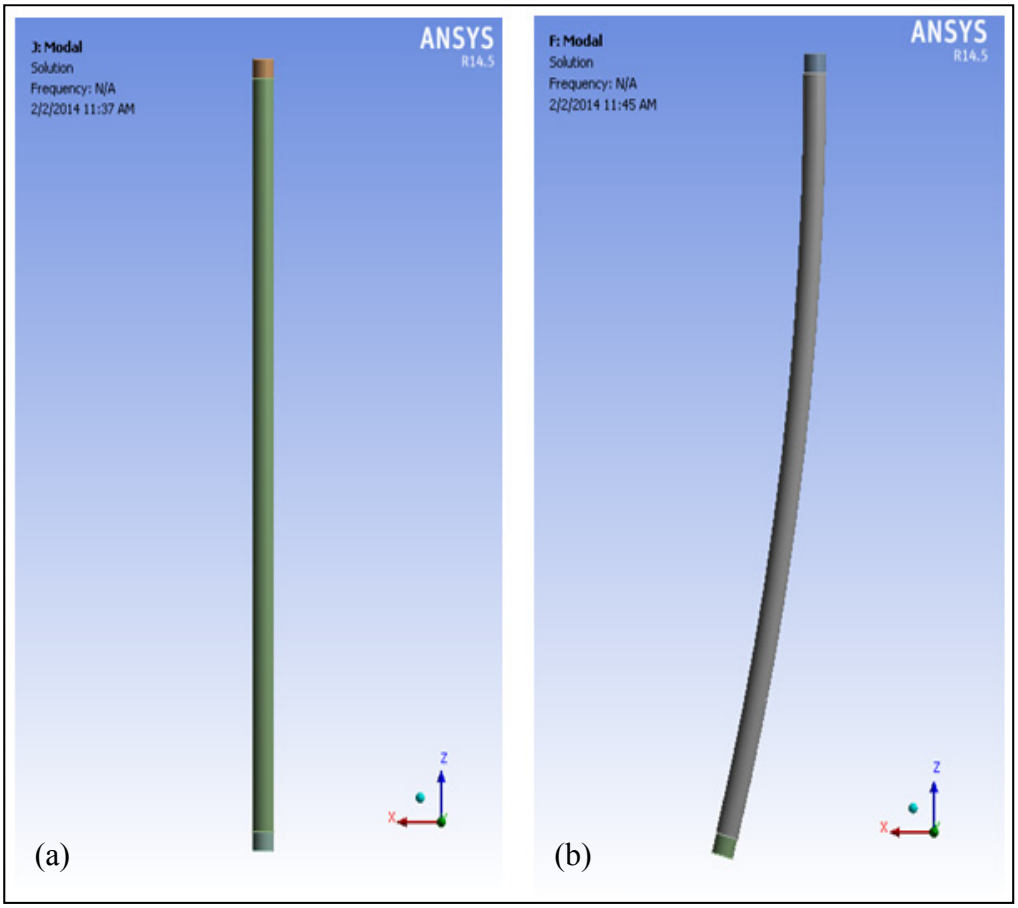

Figure 5.7 (a) Straight and (b) curved VIM models

Table 5.17 Results of straight and curved VIM models

		Straight VIM Model	Curved VIM Model	Difference %
ω_1	x-z plane	1.027 Hz	1.022 Hz	0.49
	y-z plane	1.028 Hz	1.487 Hz	44.65
ω_2	x-z plane	3.007 Hz	2.998 Hz	0.3
	y-z plane	3.01 Hz	2.989 Hz	0.7
ω_3	x-z plane	6.07 Hz	6.06 Hz	0.16
	y-z plane	6.08 Hz	6.07 Hz	0.16

Bending frequencies for each plane are specified in above table to explain the effects of the curvature clearly. It can be seen from Figure 5.7b that curvature on the VIM exists on the x-z plane. So, natural frequencies belonging to modes on this plane are denoted with the x-z plane in the table. Modes on the y-z plane which are perpendicular to curvature of the VIM are indicated with the name of the y-z plane. It is obvious that curvature contributed to the first mode only. It increased the first natural frequency on the y-z plane by a magnitude of 44.65%. On the other hand, the curved VIM and the straight beam showed the same behavior for the second and the third modes. When the test setup was considered again, it was easily seen that accelerometers were located on plane which is perpendicular to the curvature plane (Figure 5.6). Therefore, curvature is the major source of the 57% difference in the first natural frequency between theory and experiment. If the effects of the 650mm long rope and curvature which were not covered by theory are considered together, explanation of the deviation in the first natural frequency is quite clear.

The differences between the theory and the test results in terms of the second and the third natural frequencies cannot be explained with above two factors. It is obvious that their effects on these natural frequency values are infinitesimal. Geometric properties were checked again and an important point was realized. All distances between spacers in the test were assumed as constant 22cm and theoretical calculation was performed over this assumption. However, providing constant spacer distance during assembly of the VIM is not possible in reality. Assembly steps which are used to form the VIM will not be given here in detail because of the confidentiality. Only thing which should be known is that spacers are connected to each other and the distances between spacers are sustained by elastic cords. Due to the nature of the elastic cords, there is always a tolerance on spacer distances. These cords are installed and the distances are adjusted before putting the spacers into the hose. They are fastened to spacers with a pre-tension. That`s why, the tolerance on spacer distance may not exceed the value of ± 3cm. In order to understand the effect of the spacer distances, four new calculations were performed by using the modified method in Chapter 3. The first calculation

was conducted with 19cm spacer distance and then the calculation was repeated with 20.5cm, 23.5cm and 25cm spacer distances, respectively. Results of these two calculations are given in Table 5.18.

Table 5.18 VIMs with different spacer distances

	19cm Spacer Distance	**20.5cm Spacer Distance**	**22cm Spacer Distance (Nominal Value)**	**23.5cm Spacer Distance**	**25cm Spacer Distance**
ω_1	1.993 Hz	1.857 Hz	1.744 Hz	1.621 Hz	1.564 Hz
ω_2	4.543 Hz	4.119 Hz	3.77 Hz	3.465 Hz	3.229 Hz
ω_3	8.491 Hz	7.615 Hz	6.892 Hz	6.296 Hz	5.765 Hz

Although the spacer distance affects all bending natural frequencies, rates of increase in the frequency values are a little bit more for the second and the third than the first. Natural frequencies increase with decreasing spacer distance or vice versa. If the spacer distances are assumed as 20.5cm, the difference between the second and the third natural frequencies of the theory and experiment will be considerably low. Therefore, incoherencies in the second and the third frequencies can be explained with the uncertainties in the spacer distances.

In the light of the above analyses and calculations, questions about why the error ratios between theory and real structure are high have been answered with logical reasons. Rope boundary condition and the curved form of the VIM highly increased the first natural frequency whereas they did not influence the second and the third. On the other hand, dimensional instabilities of the distances between spacers could be shown as the main reason of the differences in the both second and third bending natural frequencies.

CHAPTER 6

SUMMARY AND CONCLUSIONS

In this thesis, a new theoretical method was tried to find out bending natural frequencies of the vibration isolation module (VIM) of the towed array. Viscoelastic material behavior was studied due to outer hose of the VIM. By performing a modal test on actual VIM structure, validity of the method was investigated. Additionally, effects of the boundary conditions and geometrical properties on bending natural frequencies were studied.

Towed array is generally utilized for explorations on seabed and detection of enemy threats such as torpedo or submarine. It is towed by a surface ship or a submarine and works in the water. Towed array can be several hundreds of meters and composes of mechanical and electro-mechanical components. The most important part of the towed array is the acoustic (hydrophone) section. Many hydrophones are set linearly within this section. Working principle of the array is to collect the reverberated acoustical signals from objects by means of hydrophones. Due to inherent properties of the hydrophones, any noise around them during operation diminishes the performance of the array. One of the noise sources is transverse vibrations coming over tow cable and drogue rope. So that, a component called vibration isolation module (VIM) is placed to both forward and aft ends of the acoustic section. Using indiscriminate design for the VIM may make the performance of the array worse instead of enhancing. Therefore, prediction of the dynamic behavior of the VIM before manufacture is critical to be able to define appropriate VIM structure for working frequency range. With this study, it was primarily aimed to introduce an easy and quick solution to find out bending natural frequencies of the VIM to exploit as a design tool.

Firstly, all noise mechanisms that affect the performance of the hydrophones were investigated in short. They are classified into four main groups which are ambient, radiated, flow and vibration noise. These classifications are carried out according to characteristics of the noise sources. Flow noise and vibration noise out of the four main groups have importance. Flow noise is dominant at high tow speeds within the high frequency band whereas vibration noise suppresses all kinds of noise at low tow speeds within the low frequency band. By using some statistical methods over collected data from hydrophones, flow noise can be considerably filtered out. However, this method is not applicable for vibration noise because vibration noise data can be disparate at the end of each operation condition. When the vibration noise is examined in detailed, tow cable and drogue rope vibrations are admittedly main sources of the vibration noise. Thus, only way to eliminate or minimize the vibration induced noise is to cut direct connections of the both tow cable and drogue rope with the hydrophone section. For this reason, VIMs are highly required for towed arrays.

Wide range of VIM design has been handled. Although there exists some distinctive VIM design, the general concept is usually the same. Viscoelastic outer hose, termination parts at each end, filling material, strength members and inner rigid elements are the components of the VIM. Differences between VIMs in most cases are based on either fill material or connection of inner rigid elements. For instance, some designers used solid materials, such as foam, to fill the void inside the hose while the some utilized oil-based fluids or gels instead. The widely used VIMs are composed of viscoelastic outer hose, metal termination parts, strength members, cylindrical solid spacers and oil-based inner fluid. These classical type VIMs are preferred in the towed array systems because of their low costs and easier installations.

A classical type of VIM was investigated in this study. In order to find out bending natural frequencies of the VIM, the well-known Myklestad`s Method was exploited. This method is one of the transfer matrix method used in vibration analysis. Original form of the method did not meet all requirements of the VIM so

that some modifications were made on the formulations. First of all, Myklestad`s Method bases on `Euler Beam Theory` and so the structure is always assumed as being slender. However, length to diameter ratio of the VIMs cannot be sufficiently high in some cases. It means that the structure obeys `Timoshenko Beam Theory`. Hence, shear deformation effects and rotational inertia must be taken into consideration during calculations. All equations were rearranged with regard to `Timoshenko Beam Theory`, again. Another interference to the method was to implement a variable axial force into the equations. This is essential because the VIM is subjected to drag force while towing in the water. With the above modifications, new transfer matrices were obtained to calculate bending natural frequencies of the VIM.

Whether the modified method works properly was verified before applying it on the real VIM structure. The first four bending natural frequencies of a steel tube were separately calculated for seven different boundary conditions. Besides, FEM solutions of each boundary condition were performed by using ANSYS software and results from modified method were compared with these FEM results. Differences between the results of two methods were extremely small therefore; the reliability of the modified method in calculating bending natural frequencies was proven smoothly. The only point to be noted about the modified method is that convergence analysis on the number of division, i.e. number of segments, should be always performed to minimize the error in results. By increasing/decreasing the number of segments, natural frequencies should be compared with previous calculation. Results are not going to be change anymore after a certain segment number. Either this number or higher must be used in calculations.

In order to observe performance of the modified Myklestad`s Method on real structures, a modal impact test was performed and test results were compared with modified Myklestad`s Method results. A classical VIM was prepared and hung to the overhead winch frame with a slim rope vertically. By this way, both free-free boundary conditions were satisfied and variable tension occurs on the test

specimen due to gravity. Peaks on FRF, coherence values and mode shapes obtained by impact test were checked for the validity of the test. Mode shapes showed the same characteristics with mode shapes of free-free beam as expected.

Before theoretical calculations, required mechanical properties of the VIM components must be known. Properties of the steel termination parts, Delrin® (polyacetal) solid spacers and inner fluid are easily attainable. However, the situation is a little bit complicated for the viscoelastic hose material. Viscoelastic materials do not have a constant and real elastic modulus as other materials. This mechanical property exists in complex form and it intensely depends on temperature and frequency. So, another test which is dynamic mechanical analysis (DMA) was performed and complex elastic modulus (dynamic modulus) of the hose was defined for desired temperatures and frequencies.

After all essential data were acquired, modified Myklestad`s Method was run for the test specimen. Boundary conditions were taken as free – free and only inertial properties of the inner fluid were taken into consideration. When the theoretical results and the test results for the first three bending natural frequencies were compared, the errors between results were surprisingly high. Whereas the errors between the second and the third natural frequencies were around the order of 10%, the first natural frequencies were considerably distinct from each other where the error is about 60%.

Above situation was abnormal thus; causes of the errors were investigated. Some FEM analyses were concluded with ANSYS software and three important outcomes were attained. Firstly, effect of the slim rope was studied. In order to simulate free – free boundary conditions, one must suspend the test specimen with a slim rope as long as possible. However, this cannot be possible in some cases. The rope which was used in the VIM test is 650mm in length. So, two kind of rope were modeled in ANSYS as longitudinal springs and modal analyses were done. The first rope model was very long and the second one had the exactly same length with the test rope. Axial stiffness's of the both springs were assigned as the axial

stiffness of the test rope. As a result of the analyses, it was observed that short rope increases the first natural frequency about magnitude of 16%. Its effects to the second and the third frequencies were about 2.5% and 0.4% respectively. Secondly, effect of the geometrical shape of the whole VIM structure was studied. Because of the storage condition of the hose, there was a noticeable curvature on the VIM. In order to simplify the analyses and see only the curvature effects on natural frequencies, a straight and a curved tube were modeled in ANSYS. After the modal analyses, the answer of why the first natural frequencies of the test and the modified Myklestad`s method are so different came up. It was realized that structure becomes stiffer for only the first natural frequency in perpendicular plane to curvature plane. The difference between the first frequencies of the straight beam and curved beam was about 44%. However, other natural frequencies were affected by curvature in negligible amount. During the VIM test, accelerometers were placed on the stiffer plane side. Therefore, the hanging rope and the curvature analyses clearly explain the differences in the first natural frequency when the theoretical and the test results were compared. The last investigation was focused on the spacer distance in the hose. Before the assembly of the VIM, spacer distance was defined as 22cm and all solid spacers were aligned according to this value. However, solid spacer can slip in a tolerance of ±3cm during the assembly. The first theoretical calculations were handled according to 22cm spacer distance therefore; new calculations were repeated with smaller and larger spacer distances. It was observed that 1.5 cm deviation in spacer distances causes big error between theory and the real structure. In case of the 20.5cm spacer distance, error of the modified method in both the second and the third natural frequencies becomes only 2.5%.

In conclusion, modified Myklestad`s method gives pretty good results in bending natural frequencies of the VIM structure if the boundary and geometric conditions are well-defined. Additionally, effects of the suspension rope and the curvature on the structure were investigated properly. It was obtained that short rope and curvature increase only the first natural frequency considerably. Also, spacer

distances are important parameters which affect the modal parameters of the classical VIM, directly.

This form of the modified Myklestad`s method is not adequate to identified the natural frequencies of the VIM in special cases above. However, this method can be utilized to parametric studies to perceive how the natural frequencies will change. In the future, suspension rope can be added into the method as a boundary condition. Additionally, stiffness effect of the curvature in one direction can be modeled with virtual torsional springs. In order to simulate the sea conditions, both real lift and drag forces can be also added to equations. After the above extra modifications, test should be performed on the VIM either as hung or being towed in water.

REFERENCES

[1] Li Q., 2012, Digital Sonar Design in Underwater Acoustics, Zhejiang University Press.

[2] Dowling A. P., 1988, "The Dynamics of Towed Flexible Cylinders Part1. Neutrally Buoyant Elements," Journal of Fluid Mechanics, 187, pp. 507–532.

[3] Payne C. M., 2006, Principle of Naval Weapon Systems, Naval Institute Press.

[4] Gill T. G., and Morningstar C. L., 1994, "Vibration Isolation Module for Towed Hydrophone Streamer," United State Patent, (US5367499 A).

[5] Lasky M., Doolittle R. D., Simmons B. D., and Lemon S. G., 2004, "Recent Progress in Towed Hydrophone Array Research," IEEE Journal of Oceanic Engineering, 29(2), pp. 374–387.

[6] Wenz G. M., 1962, "Acoustic Ambiant Noise in the Ocean: Spectra and Sources," Journal of the Acoustical Society of America, 34(12), pp. 1936–1956.

[7] Urick R. J., 1983, Principle of Under Water Sound, McGraw-Hill, New York.

[8] Hodges R. P., 2010, Underwater Acoustics Analysis, Design and Performance of Sonar, John Wiley & Sons.

[9] Elboth T., Lilja D., Reif B. A. P., and Andreassen O., 2010, "Investigation of Flow and Flow Noise Around a Seismic Streamer Cable," Geophysics, 75(1), pp. Q1–Q9.

[10] Ketchman J., 1981, "Vibration Induced in Towed Linear Underwater Array Cables," IEEE Journal of Oceanic Engineering, OE-6(3), pp. 77–87.

[11] Miller H. A., Smith R. R., and Nichols C. S., 1978, “Solid Filled Vibration Isolation Module For a Towed Sonar Array,” United State Patent, (US4090168 A).

[12] Appling J., 1986, “Vibration Isolation Module,” United State Patent, (US4628851 A).

[13] McGowan G. A., and MacClloch D. B., 1987, “Vibration Isolation Module for Sonar Towed Arrays,” United State Patent, (US4660183 A).

[14] Carpenter A. L., and Adkins M. W., 1995, “Vibration Isolation Module,” United State Patent, (US5463193 A).

[15] Cameron N. W., and Parsons A. T., “Vibration Isolation Section for a Seismic Streamer,” European Patent Office, (EP0171936 A2), p. Feb. 19, 1986.

[16] Reynier R., Malcor J. G., Moresco G., and Ramoger F., 1988, “Vibration Damper for a Towed Body,” United State Patent, (US4762208 A).

[17] Andrews D. E., 1991, “Vibration Isolation Module for Towed Seismic Arrays,” United State Patent, (US5062085 A).

[18] Harvey A. P., 1995, “Vibration Isolation Modules (VIM) for Towed Arrays Streamers,” United State Patent, (US5471436 A).

[19] Païdoussis M. P., 1965, “Vibration of Flexible Cylinders With Spported Ends, Induced by Axial Flow,” Proceedings of the Institution of Mechanical Engineers, 180(310), pp. 268–279.

[20] Païdoussis M. P., 1970, “Dynamics of Submerged Towed Cylinders,” Eighth Symposium on Naval Hydrodynamics, (Session VIII).

[21] Païdoussis M. P., Grinevich E., Adamovic D., and Semler C., 2002, “Linear and Nonlinear Dynamics of Cantilevered Cylinders in Axial Flow. Part 1: Physical Dynamics,” Journal of Fluids and Structures, 16(6), pp. 691–713.

[22] Lopes J. L., Païdoussis M. P., and Semler C., 2002, "Linear and Nonlinear Dynamics of Cantilevered Cylinders in Axial Flow. Part 2:The Equation of Motion," Journal of Fluids and Structures, 16(6), pp. 715–737.

[23] Semler C., Lopes J. L., Augu N., and Païdoussis M. P., 2002, "Linear and Nonlinear Dynamics of Cantilevered Cylinders in Axial Flow. Part 3:Nonlinear Dynamics," Journal of Fluids and Structures, 16(6), pp. 739–759.

[24] De Langre E., Païdoussis M. P., Doaré O., and Modarres-Sadeghi Y., 2007, "Flutter of Long Flexible Cylinders in Axial Flow," Journal of Fluid Mechanics, 571, pp. 371–389.

[25] Bhattacharyya S. K., Vendhan C. P., and Sudarsan K., 2000, "The Finite Element Method For Hydroelastic Instability of Underwater Towed Cylindrical Structures," Journal of Sound and Vibration, 237(1), pp. 119–143.

[26] Dowling A. P., 1988, "The Dynamics of Towed Flexible Cylinders Part 2. Negatively Buoyant Ellements," Journal of Fluid Mechanics, 187, pp. 533–571.

[27] Doshi C. S., 1979, "On the Analysis of the Timoshenko Beam Theory With and Without Internal Damping," Rochester Institute of Technology.

[28] Loudini M., Boukhetala D., Tadjine M., and Boumehdi M. A., 2006, "Application of Timoshenko Beam Theory for Deriving Motion Equations of a Lightweight Elastic Link Robot Manipulator," ICGST-ARAS Journal, 5(2).

[29] Robinson B. J., 2009, "Characterization of the Viscoelastic Behavior of Pharmaceutical Powders," Philadelphia, USA, Drexel University.

[30] Banks H. T., Hu S., and Kenz Z. R., 2011, "A Brief Review of Elasticity and Viscoelasticity for Solids," Adv. Appl. Math. Mech., 3(1), pp. 1–51.

[31] Balmes E., 2006, “Modeling Damping at the Material and Structure Levels.”

[32] Fertis D. G., 1995, Mechanical and Structural Vibrations, Wiley, New York.

[33] Tse F. S., 1978, Mechanical Vibrations: Theory and Applications, Allyn and Bacon, Boston.

[34] Beer F. P., 2006, Mechanics of Materials, McGraw-Hill Higher Education, Boston.

[35] Wu J.-S., and Chen C.-T., 2007, “A Lumped-Mass TMM for Free Vibration Analysis of a Multi-Step Timoshenko Beam Carrying Eccentric Lumped Masses with Rotary Inertias,” Journal of Sound and Vibration, 301(3-5), pp. 878–897.

[36] Sule S., 2011, “Approximate Method for the Determination of Natural Frequencies of a Multi-Degree of Freedom Beam Systems,” Nigerian Journal of Technology, 30(2).

[37] Minhinnick I. T., 1956, The Theoretical Determination of Normal Modes and Frequencies of Vibration, Ministery of Supply.

[38] Al-Bahkali E., and ElMadany M., 2004, “Dynamic Analysis of Rotating Machinery Using Computer Aided Design Approach,” Saudi Arabia, pp. 192–201.

[39] Darlow M. S., Murphy B. T., Elder J. A., and Sandor G. N., 1980, “Extension of the Transfer Matrix Method for Rotordynamic Analysis to Include a Direct Representation of Conical Sections and Trunnions,” Journal of Mechanical Design, 102(1), p. 122.

[40] Nakano A., 1971, Application of Transfer Matrix Method to the Structural Dynamics of Rocket Vehicles, Institute of Space and Aeronautical Science, University of Tokyo.

[41] Chen L.-Q., and Ding H., 2010, "Steady-State Transverse Response in Coupled Planar Vibration of Axially Moving Viscoelastic Beams," Journal of Vibration and Acoustics, 132(1), p. 011009.

[42] West R. A., 1992, "Damping of Elastic-Viscoelastic Beams," Rochester Institute of Technology.

[43] 2001, Handbook of Materials Behavior Models, Academic Press, San Diego, CA.

[44] Petkova S., Kisliakov D., and Yordanov Y., 2011, "Transverse Earthquake-Induced Vibrations of a Buried Pressure Pipeline Including Fluid–Structure Interaction," Journal of Theoretical and Applied Mechanics, 41(2), pp. 49–68.

[45] Wiggert D. C., and Tijsseling A. S., 2001, "Fluid Transients and Fluid-Structure Interaction in Flexible Liquid-Filled Piping," Applied Mechanics Reviews, 54(5), p. 455.

[46] Huang W., Liao M., and Cheng Y., 2012, "Combined Method with Transfer Matrix and Measurement for Investigating the Dynamic Behavior of Wind Turbine Tower," IEEE, pp. 1–6.

[47] Schwarz B. J., and Richardson M. H., 1999, "Experimental Modal Analysis," CSI Reliability Week.

APPENDIX

DYNAMIC MODULUS GRAPHS

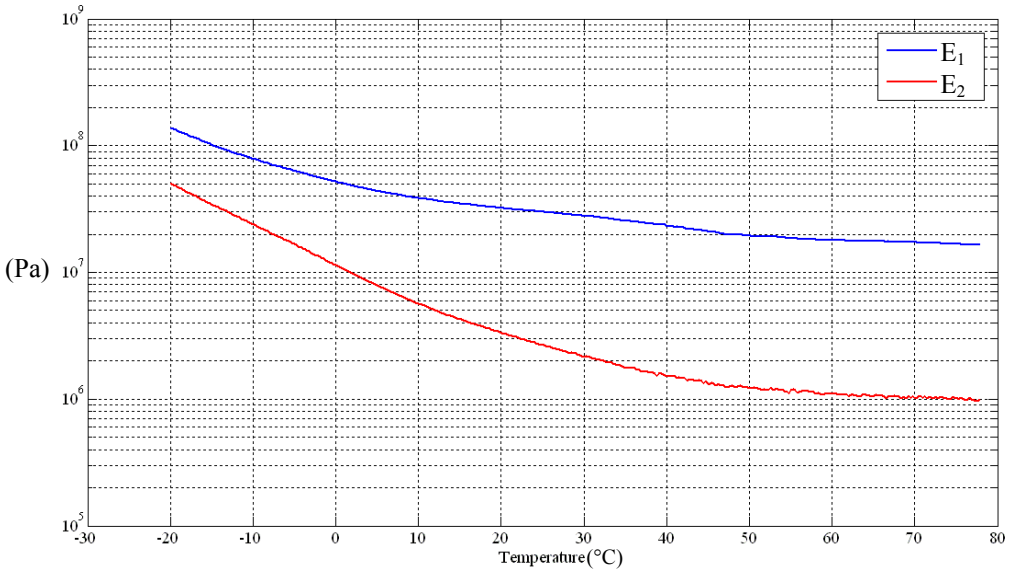

Figure A1 Storage (E_1) and Loss modulus (E_2) of the hose vs. temperature at constant frequency of 1Hz

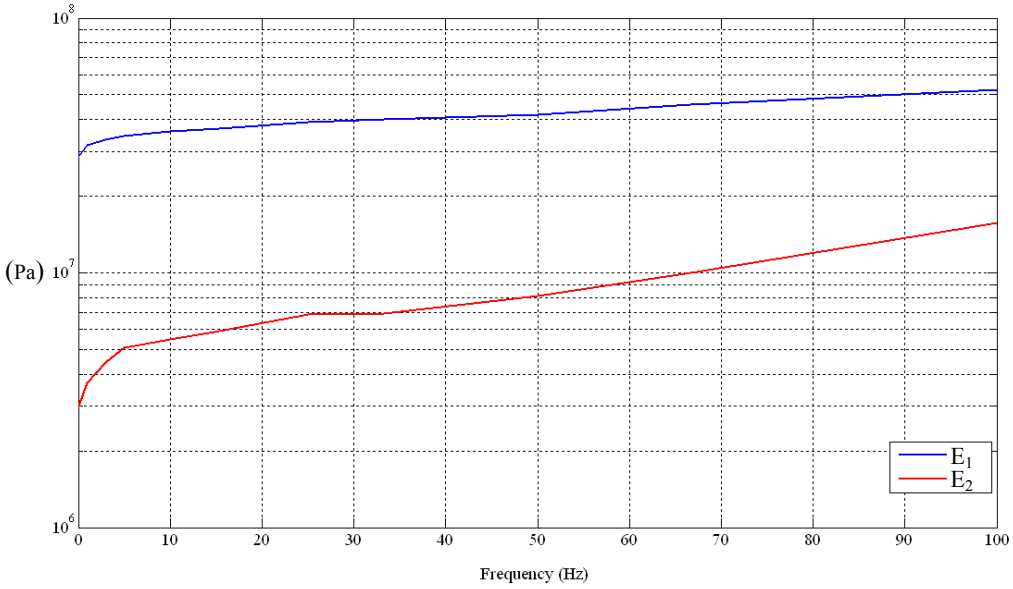

Figure A2 Storage (E_1) and Loss modulus (E_2) of the hose vs. frequency at constant temperature of 23 °C